1998-09

Comparison of advanced Arctic Ocean model sea ice fields to satellite derived measurements

Dimitriou, David S.

Monterey, California. Naval Postgraduate School

DUDLEY KNOX LIBRARY
NAVAL POSTGRADUATE SCHOOL
MONTEREY CA 93943-5101

NAVAL POSTGRADUATE SCHOOL
Monterey, California

THESIS

COMPARISON OF ADVANCED ARCTIC OCEAN MODEL SEA ICE FIELDS TO SATELLITE DERIVED MEASUREMENTS

by
David S. Dimitriou

September 1998

Thesis Advisor: Yuxia Zhang
Co-Advisor: Albert J. Semtner

REPORT DOCUMENTATION PAGE

Form Approved OMB No. 0704-0188

1. AGENCY USE ONLY *(Leave blank)*	2. REPORT DATE	3. REPORT TYPE AND DATES COVERED
	September 1998	Master's Thesis

4. TITLE AND SUBTITLE
COMPARISON OF ADVANCED ARCTIC OCEAN MODEL SEA ICE FIELDS TO SATELLITE DERIVED MEASUREMENTS

5. FUNDING NUMBERS

6. AUTHOR(S)
Dimitriou, David S.

7. PERFORMING ORGANIZATION NAME(S) AND ADDRESS(ES)
Naval Postgraduate School
Monterey, CA 93943-5000

8. PERFORMING ORGANIZATION REPORT NUMBER

9. SPONSORING / MONITORING AGENCY NAME(S) AND ADDRESS(ES)

10. SPONSORING / MONITORING AGENCY REPORT NUMBER

11. SUPPLEMENTARY NOTES
The views expressed in this thesis are those of the author and do not reflect the official policy or position of the Department of Defense or the U.S. Government.

12a. DISTRIBUTION / AVAILABILITY STATEMENT
Approved for public release; distribution is unlimited.

12b. DISTRIBUTION CODE

13. ABSTRACT *(maximum 200 words)*

Numerical models have proven integral to the study of climate dynamics. Sea ice models are critical to the improvement of general circulation models used to study the global climate. The object of this study is to evaluate a high resolution ice-ocean coupled model by comparing it to derived measurements from SMMR and SSM/I satellite observations. Utilized for this study was the NASA Goddard Space Flight (GSFC) Sea Ice Concentration Data Set from the National Snow and Ice Data Center. Using animations of side-by-side presentations, variability comparisons and anomaly values the of similarities and differences between the model and the satellite were noted. The model shows a true representation of the seasonal cycle of ice concentration variation, with natural growth, advection, decay. Model performance is weakest in the East Siberian and Laptev Seas where excessive ice is developed. A 30 day lag in the freezing and melting of ice in Hudson Bay was noted in the model. The use of monthly mean Levitus temperatures adversely affects model performance evidenced by a tendency to grow and retain excess ice in the marginal seas of the Arctic Ocean.

14. SUBJECT TERMS	15. NUMBER OF PAGES
	72
	16. PRICE CODE

17. SECURITY CLASSIFICATION OF REPORT	18. SECURITY CLASSIFICATION OF THIS PAGE	19. SECURITY CLASSIFI- CATION OF ABSTRACT	20. LIMITATION OF ABSTRACT
Unclassified	Unclassified	Unclassified	UL

NSN 7540-01-280-5500

Standard Form 298 (Rev. 2-89)
Prescribed by ANSI Std. 239-18

Approved for public release; distribution is unlimited

COMPARISON OF ADVANCED ARCTIC OCEAN MODEL SEA ICE FIELDS TO SATELLITE DERIVED MEASUREMENTS

David S. Dimitriou
Lieutenant, United States Navy
B.S., University of Washington, 1989

Submitted in partial fulfillment of the
requirements for the degree of

MASTER OF SCIENCE IN METEOROLOGY AND PHYSICAL OCEANOGRAPHY

from the

NAVAL POSTGRADUATE SCHOOL
September 1998

ABSTRACT

Numerical models have proven integral to the study of climate dynamics. Sea ice models are critical to the improvement of general circulation models used to study the global climate. The object of this study is to evaluate a high resolution ice-ocean coupled model by comparing it to derived measurements from SMMR and SSM/I satellite observations. Utilized for this study was the NASA Goddard Space Flight (GSFC) Sea Ice Concentration Data Set from the National Snow and Ice Data Center. Using animations of side-by-side presentations, variability comparisons and anomaly values of the similarities and differences between the model and the satellite were noted. The model shows a true representation of the seasonal cycle of ice concentration variation, with natural growth, advection, decay. Model performance is weakest in the East Siberian and Laptev Seas where excessive ice is developed. A 30 day lag in the freezing and melting of ice in Hudson Bay was noted in the model. The use of monthly mean Levitus temperatures adversely affects model performance evidenced by a tendency to grow and retain excess ice in the marginal seas of the Arctic.

TABLE OF CONTENTS

I. INTRODUCTION

Numerical models have proven to be invaluable tools in the study of the global climate. Among them, the coupled sea ice-ocean models provide a critical element to the understanding of global climatology. Navy leaders, recognizing the importance of oceanography, specifically the understanding of the arctic to the success of Naval Operations, have stated that oceanographic research is critical to the Navy mission. For continued successful operations in the arctic and worldwide it is essential that the Navy continue to support the development and improvement of ice-ocean models.

In an otherwise data sparse region satellite sensors provide a unique way in which to validate sea ice-ocean models. The radiance values returned by SMMR (Scanning Multichannel Microwave Radiometer) and SSM/I (Special Sensor Microwave/Imager) sensors have been converted to ice concentration values using the NASA (National Aeronautics and Space Administration) team algorithm (Cavalieri et al., 1984; Gloerson and Cavalieri, 1986). This concentration data set provides an invaluable source of information about the variability in the formation, decay and areal extent of

arctic sea ice. The comparison of this satellite-derived data with model simulations will show similarities and differences, which are the keys to understanding the strengths and weaknesses of ice models.

The objective of this paper is to compare the observed data from SMMR & SSM/I with the model simulation output. This study will include the entire arctic basin with focus on regional features such as the shallow water Kara and Barents Seas and Hudson Bay. The hope is that by using the comparison of model simulations against observational data a better understanding of how models reflect actual conditions will be obtained. With improved modeling tools the Arctic Ocean and its importance to global climate will be better understood. The desired result is to bring the model into closer agreement with nature by comparing it with observational data.

This paper is organized as follows: Chapter I, this introduction. Chapter II is a presentation of the importance of the arctic to the global climate, the use of numerical modeling to study this area and why the Navy is concerned with this problem. Chapter III contains a complete discussion of the SMMR & SSM/I data set used to validate the model and the manipulations involved in processing the data set. Chapter IV discusses the model that is being evaluated

by this paper and the initializations and forcings utilized for this specific simulation. Chapter V will show the results of side by side comparisons of the 15-year model simulation with SMMR & SSM/I observations, followed by comparison of model variability to SMMR & SSM/I variability values and the model output compared to SMMR & SSM/I as an anomaly. Chapter VI concerns itself with the discussion of recommended areas of further studies; considerations for new model simulations using the information learned by this study and the suggested ways to improve on numerical modeling of the arctic.

II. THE ROLE OF THE ARCTIC

The Arctic has long been recognized both as a key indicator of global warming and as an integral component of the global climate-modeling problem. General circulation models (GCMs) predict a strong signal in the arctic in response to CO_2-induced global warming. These global models predict extensive thinning and retreat of the arctic ice especially in the late fall and winter (Mitchell et al., 1990). This response by the ice will serve to contribute to a positive snow-ice albedo feedback mechanism. The resultant decrease in snow-ice coverage will act to decrease the reflectivity and increase the absorption of solar radiation.

The Arctic Ocean directly impacts the global climate through heat balance and thermohaline circulation. Heat flux in the arctic is primarily through polynyas, leads and along the ice margins. Ice motion and deformation result in a varying spatial distribution of sea-ice thickness, leads and polynyas. The changes in arctic sea-ice directly affect the air-sea heat exchange budget (Randall et al., 1998). The growth and transport of ice out of the Arctic basin directly controls the stratification of the underlying ocean waters. This stratification precludes strong heat fluxes within the

water column beneath the ice thereby mediating any large perturbations in ice thickness and extent.

The world's oceans receive much of their deep water from the Arctic. Convective overturning of surface waters is regulated by the input of ice and fresh water from the Arctic Ocean into the North Atlantic. Convection in the Greenland and Icelandic Seas is conditioned by freshwater export from the Arctic (Aagaard and Carmack, 1994). The transport of cold fresh water from the Arctic Ocean into the North Atlantic makes the Fram St. area critical to the understanding of the global heat budget.

While general circulation models have many problems that arise from the way sea-ice and other arctic physical processes are handled, they are improving. Motivated by the high-latitude sensitivity observed in global climate models which tends to be exaggerated by incompletely modeled sea-ice processes, modelers are working to improve GCMs (Randall et al., 1998).

Naval leadership, once primarily concerned with the Arctic's strategic importance and operations beneath the ice, has recently recognized its importance on a larger scale. "The important role played by the Arctic Ocean in global climate, and the international concern for pollution

in the region, have fueled greater interest in Arctic research by civilian oceanographers."

"...the United States Navy, a global navy, must understand the global environment in which it trains and operates. To be successful a modern navy requires the very best knowledge of oceanography and its related sciences."

"A robust competency in oceanography is a core requirement and responsibility of the U.S. Navy, one so vital to the success of our operations that we must lead in focusing national attention on ocean policy and programs." (ADM. Boorda, 1996) In this setting this paper will compare the observational data obtained from satellites with the output fields from a 15-year model simulation. The time series of ice concentration data will be studied to identify model strengths and weaknesses in the accurate reproduction of the complex variability of nature.

III. THE SATELLITE DERIVED DATA SET DESCRIPTION

A. DATA SET SOURCE

The data utilized in this study is the NASA GSFC (Goddard Space Flight Center) Sea Ice Concentration Data Set. Data were provided by the EOS (Earth Observing System) Distributed Active Archive Center (DAAC) at the NSIDC (National Snow and Ice Data Center), University of Colorado, Boulder, CO. via the internet by anonymous FTP.

1. SMMR and SSM/I

The sea ice concentrations are derived from Nimbus 7 SMMR and DMSP (Defense Meteorological Satellite Program) SSM/I satellite observations. Brightness temperatures observed by the satellites were processed into derived values of sea ice concentration. Two concentration measures are popularly used, ice extent and ice area. Ice extent is obtained by summing the area of each grid cell with $\geq$ 15% ice concentration. The area of sea ice is obtained by summing the ice concentration times grid cell area (Gloerson et al., 1992). Generally, the sea ice extent boundary is larger than the ice area boundary. The SMMR brightness temperatures were processed at NASA GSFC while processing of SSM/I brightness temperatures was done at NSIDC.

The Oceans and Ice Branch, Laboratory for Hydrospheric Processes at NASA GSFC generated the sea ice concentrations from the processed brightness temperatures.

2. Temporal and Spatial Coverage

The temporal and spatial coverage of the data set and description of data gaps and interpolation methods utilized are as follows. The data set begins October 26, 1978 and continues through September 30, 1995. For the period October 26, 1978 through December 01, 1987 SSMR data was collected every other day. In 1982 data gaps occur on Aug 4,8,16. In 1984 data is missing for Aug 13-23. From December 01, 1987 through September 30, 1995 SSM/I data was collected daily. Data is missing for 3 Dec 1987 - 13 Jan 1988.

The scattered pixels of missing data, resulting generally from mapping the orbital data to the SSM/I grid, were filled by applying a spatial linear interpolation scheme on the brightness temperature maps. The larger areas of missing data, resulting from gaps between orbital swaths (generally at low latitudes on daily maps) or from partial coverage or missing days were filled by temporal interpolation on sea ice concentration maps. (NSIDC, Data Set Description) No interpolation was done for the period 3 December 1987 - 13 January 1988; this remains as missing data.

Sea Ice concentration data is available for the entire Arctic and is projected on a polar stereographic grid (Fig. 3-1). However, since the data is derived from observations made by polar orbiting satellites, a spatial gap in coverage exists. The inclination of a polar orbiting satellite precludes it from passing directly over the pole. This circular gap over the pole has been masked in the presentation of data by using a polemask. The polemask for the later SSM/I data is smaller in areal extent.

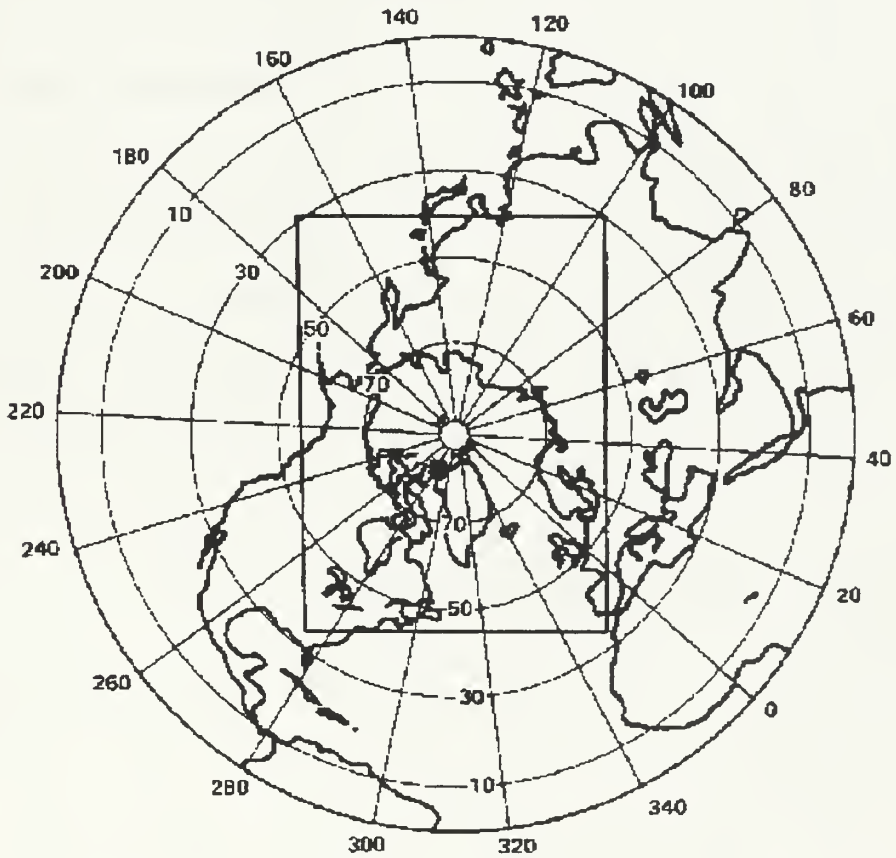

Figure 3-1. Satellite data set coverage map for the Arctic Region.

3. Grid Projection

The sea ice concentration data is presented on a 448 X 304 grid with nominal grid size of 25 km. For the purposes of this study the data was cropped to 361 X 301 to correspond with the model grid or interpolated to the model grid.

B. NASA TEAM ALGORITHM

Sea ice concentrations were derived using the NASA Team Algorithm. Cavalieri et al. [1991] outline how this algorithm uses three SSM/I channels, one each at 19.4 GHz, both horizontal and vertical polarization, and one at 37.0 GHz, vertical polarization. Two ratios of radiances from the three channels are mapped onto a polar stereographic grid and then used to calculate grids for the two independent variables used. The ratios are the polarization ratio (PR) and the spectral gradient ratio (GR).

$$PR = [TB(19V) - TB(19H)]/[TB(19V) + TB(19H)]$$
$$GR = [TB(37V) - TB(19V)]/[TB(37V) + TB(19V)]$$

where TB is the observed brightness temperature at the specified frequency and polarization. From these variables first-year (C_F) and multi-year ice (C_M) concentrations are calculated.

$$C_F = (a_0 + a_1 PR + a_2 GR + a_3 PR \cdot GR) / D$$
$$C_M = (b_0 + b_1 PR + b_2 GR + b_3 PR \cdot GR) / D$$

where $D = c_0 + c_1 PR + c_2 GR + c_3 PR \cdot GR$.

Then the total ice concentration (C_T) is calculated as the sum of the first and multi-year concentrations:

$$C_T = C_F + C_M .$$

The coefficients a_i, b_i, and c_i(I=0,3) are functions of a set of nine TBs. These act as algorithm tie-points to connect the SSM/I radiances to areas of known ice concentrations for each of the three SSM/I channels.

C. DATA CONFIDENCE

The satellite data set used in this study is not considered to be ground truth measurements of ice concentrations but rather a well-known set of observations with understood biases and errors. In order to evaluate model performance using satellite data a measure of satellite data quality must be provided. In 1987 NASA initiated the sea ice validation program (Cavalieri and Swift, 1987). This program was designed to provide the user with a measure of the precision and accuracy of the derived sea ice products. The study used comparisons of SSM/I derived ice concentrations with those obtained from Landsat imagery and aircraft underflights of the SSM/I satellites. The study concluded that

the Landsat imagery accuracy was 4%. The SSM/I-Landsat comparisons show that under wintertime conditions SSM/I has an accuracy of 7% with a negative bias of 4%. This suggests that SSM/I underestimates the sea ice concentration relative to Landsat (Steffen and Schweiger, 1991). Larger errors were observed for summer melt conditions where the mean difference was 11%, and the standard deviation as high as 22%. The study also indicates that where aircraft underflight observations for areas of 100% ice concentration (aircraft) have SSM/I values of 97.6% ± 2.4%. This validation study gives confidence in the value and accuracy of SSM/I-derived ice concentration products. Cavalieri [1991] reports that the SSM/I validation can also be extended to SMMR sea ice data because a comparison (P. Gloerson, unpublished data, 1991) has shown that concentration differences (SMMR-SSM/I) during the two months of coverage overlap are 0.5% ±5% during the boreal summer.

IV. MODEL DESCRIPTION

The high-resolution coupled ice-ocean Arctic model used in this study employs an elastic-viscous-plastic (EVP) rheology (Hunke and Dukowicz, 1997). The ice thermodynamics is determined from an energy budget at the ice surface following Parkinson and Washington (1979) and the zero-layer approximation of Semtner (1976) for heat conduction through the ice. The Semtner/Chervin free surface model modified for the Arctic (Semtner and Chervin, 1992; Maslowski, 1997) with an added free-surface (Killworth et al., 1991) which allows unsmoothed bathymetry was used for the ocean.

The specific model simulation evaluated in this study used ECMWF (European Center for Medium-range Weather Forecasting) reanalysis fields. The ocean model was run stand-alone for seven years using Levitus (Levitus, 1982) salinity and temperatures for initialization. In the first year ECMWF 1992 annual wind stresses were used. The following six years used three-day averaged 1992 wind stress fields to force the model (Maslowski, 1997).

The ice model was run stand-alone for six years with an assumed initial ice thickness of 2 m, and the ice surface temperature at the freezing point. The three-day averaged

1992 operational ECMWF sea level pressure and heat fluxes were used as the atmospheric forcing and the seventh year three-day snapshot of the ocean model output as the oceanic forcing. The coupled ice-ocean model was run for five years with 1990-94 three-day averaged operational ECMWF sea level pressure and heat fluxes for atmospheric forcing.

After the 12-year initialization run the coupled ice-ocean model was run for an additional 15 years using daily averaged (1979-93) ECMWF reanalysis fields. Input variables were the 10 m winds, incoming longwave and short-wave radiations, surface air temperature and dewpoint. The ocean model surface layer utilized a relaxation scheme to Levitus and Boyer [1994] salinity and temperature on a 90 day time scale. The relaxation scheme for the surface layer of the ocean model to Levitus changes the primitive equation for temperature tracer (Parsons, 1995) as follows:

$$\frac{\partial T}{\partial t} + L(T) = D_V \frac{\partial^2 T}{\partial z^2} + D_h \nabla_H^4 (T) + \frac{1}{90(86{,}400)}(T - T_{LEV})$$

with $T_{LEV} = T_N - \alpha * (T_N - T_{N+1})$

where N = Levitus monthly mean, and N from 1 to 12

with α = weight from 0.0 to 1.0 incremented on 40 minute time step over monthly time scale.

(D_h, D_v) = (Horizontal, Vertical) eddy diffusivity coefficients.

salinity is handled similarly.

The model output is on a polar stereographic grid of 361 X 301 resulting in a nominal resolution of 18 km.

V. SATELLITE OBSERVATIONS AND MODEL COMPARISON

In order to use the satellite observation data files for comparison with the model output fields they first had to be put into a compatible format. The raw binary daily satellite observation files were converted to the netCDF format which the model output fields were stored in. The model output consists of annual files with time frames every 3 days. The satellite data set, however, consists initially of observations every other day and subsequently daily observation files. The satellite observation annual files were created with 121 or 122 frames each, to match the model output. When the satellite observation date corresponded with the model date, it was used directly. In the cases where the satellite observation date did not match the model date, the satellite observations one day before and one day after the model date were interpolated.

A. SIDE-BY-SIDE ANIMATION

The annual model and satellite netCDF files were displayed side-by-side (Fig. 5-1) in a tandem panel presentation and appended to create a 15-year movie with a date timestamp and color key for ice concentration percentage.

The side by side animation of model and satellite fields allows visual comparison of ice concentration and the advance/retreat of the ice edge. Additionally, the animation provides an excellent tool for observing the effects of weather events on ice concentration. In this section, several examples are given to demonstrate how well the model simulates the seasonal variation, small-scale features and the effects of atmospheric circulation.

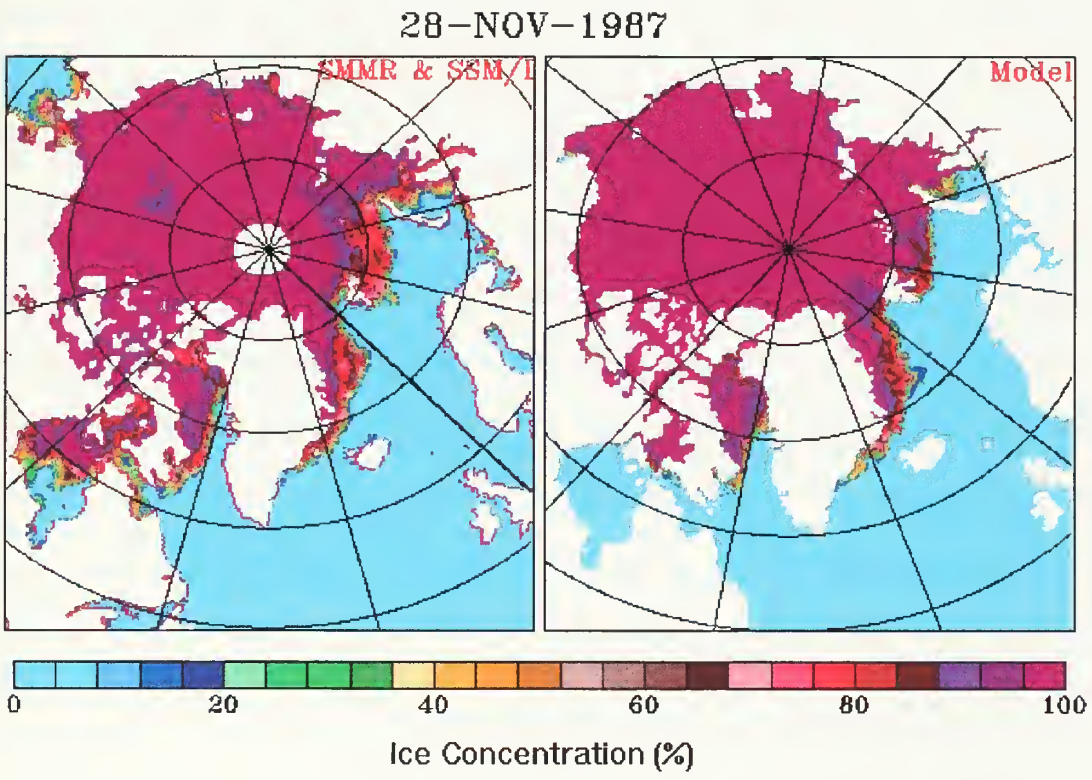

Figure 5-1. Representative single frame from 15-year side-by-side animation of satellite observed (left) and model simulated (right) ice concentrations (%).

1992 operational ECMWF sea level pressure and heat fluxes were used as the atmospheric forcing and the seventh year three-day snapshot of the ocean model output as the oceanic forcing. The coupled ice-ocean model was run for five years with 1990-94 three-day averaged operational ECMWF sea level pressure and heat fluxes for atmospheric forcing.

After the 12-year initialization run the coupled ice-ocean model was run for an additional 15 years using daily averaged (1979-93) ECMWF reanalysis fields. Input variables were the 10 m winds, incoming longwave and short-wave radiations, surface air temperature and dewpoint. The ocean model surface layer utilized a relaxation scheme to Levitus and Boyer [1994] salinity and temperature on a 90 day time scale. The relaxation scheme for the surface layer of the ocean model to Levitus changes the primitive equation for temperature tracer (Parsons, 1995) as follows:

$$\frac{\partial T}{\partial t} + L(T) = D_V \frac{\partial^2 T}{\partial z^2} + D_h \nabla_H^4 (T) + \frac{1}{90(86{,}400)} (T - T_{LEV})$$

with $T_{LEV} = T_N - \alpha * (T_N - T_{N+1})$

where N = Levitus monthly mean, and N from 1 to 12

with α = weight from 0.0 to 1.0 incremented on 40 minute time step over monthly time scale.

(D_h, D_v) = (Horizontal, Vertical) eddy diffusivity coefficients .

salinity is handled similarly.

The model output is on a polar stereographic grid of 361 X 301 resulting in a nominal resolution of 18 km.

V. SATELLITE OBSERVATIONS AND MODEL COMPARISON

In order to use the satellite observation data files for comparison with the model output fields they first had to be put into a compatible format. The raw binary daily satellite observation files were converted to the netCDF format which the model output fields were stored in. The model output consists of annual files with time frames every 3 days. The satellite data set, however, consists initially of observations every other day and subsequently daily observation files. The satellite observation annual files were created with 121 or 122 frames each, to match the model output. When the satellite observation date corresponded with the model date, it was used directly. In the cases where the satellite observation date did not match the model date, the satellite observations one day before and one day after the model date were interpolated.

A. SIDE-BY-SIDE ANIMATION

The annual model and satellite netCDF files were displayed side-by-side (Fig. 5-1) in a tandem panel presentation and appended to create a 15-year movie with a date timestamp and color key for ice concentration percentage.

The side by side animation of model and satellite fields allows visual comparison of ice concentration and the advance/retreat of the ice edge. Additionally, the animation provides an excellent tool for observing the effects of weather events on ice concentration. In this section, several examples are given to demonstrate how well the model simulates the seasonal variation, small-scale features and the effects of atmospheric circulation.

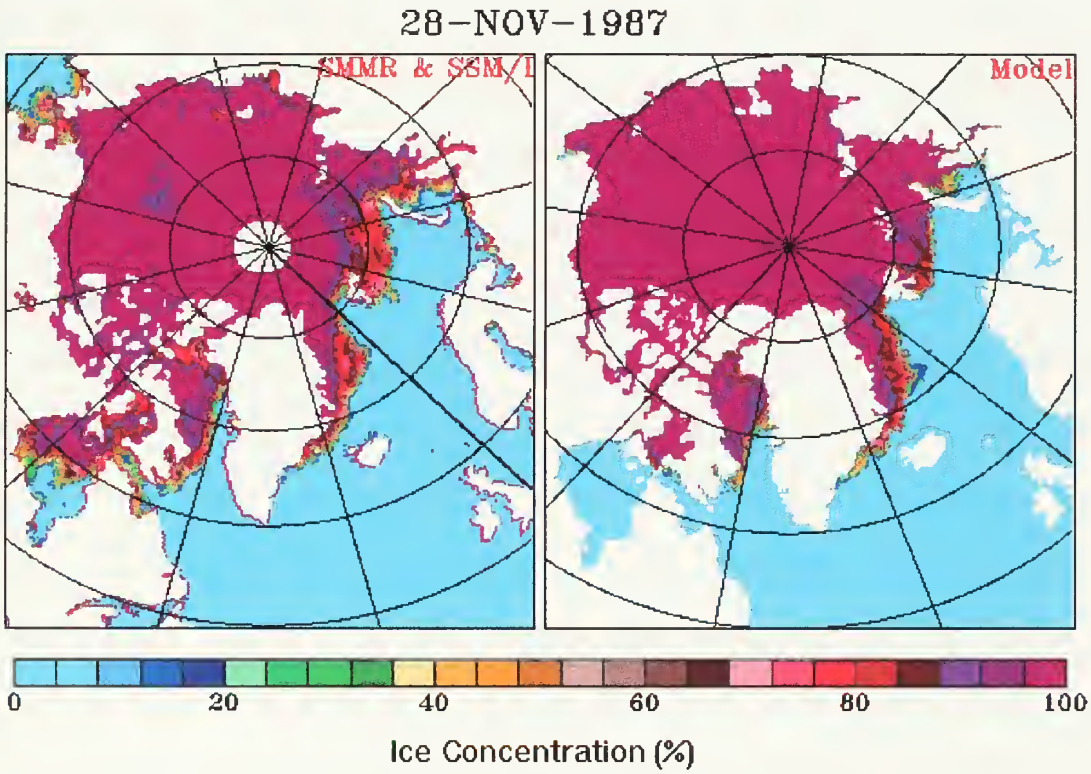

Figure 5-1. Representative single frame from 15-year side-by-side animation of satellite observed (left) and model simulated (right) ice concentrations (%).

1. Seasonal Variation

In this section and others that follow, the analysis and discussion is based on a review of the animation and overall impressions and conclusions are then formulated. Figures are presented only for particular events or regional analysis. The model accurately depicts the annual variation of ice concentration with growth beginning in the fall to maximum extent and concentration in the winter. In late spring the model accurately depicts the decay and shrinking of the ice extent to a minimum in summer. Throughout the 15-year model simulation the seasonal variation of ice extent is well depicted. However, the model tends to be somewhat slow in both the freezing and melting of sea ice, lagging behind the observed satellite growth and decay. Model depictions of areas shown by satellite imagery to have become ice-free continue to show that ice is present. The model also depicts areas as ice free when satellite observations show them beginning to experience ice growth. These problems are mainly restricted to the marginal seas surrounding the central arctic. The model consistently depicts the central Arctic ice concentrations very favorably to observations.

The Hudson Bay region provides an excellent example of how the model does a good job of simulating the seasonal

variation in ice content but lags behind satellite observations temporally (Fig. 5-2). The model does a good job of portraying the formation of ice in Hudson Bay with the freezing typically starting in the northern end of the bay and progressing southward until the entire bay is frozen over. Satellite observations show that Hudson Bay usually will freeze over by mid-November. This is repeated over the 15-year study with some small inter-annual variability. The model is consistently late in its freezing of Hudson Bay by approximately 30 days. Figure 5-2 depicts an example of the 30-day delay in the model. The satellite observations show Hudson Bay to be frozen by 15 November but complete freeze-up by the model is delayed until about 15 December. Not shown is that by mid January the model has caught up to satellite observations and shows the bay entirely frozen. In May ice begins to melt and concentration values are reduced in the eastern portion of the bay in both satellite and model fields. The satellite observations show Hudson Bay to be free of ice by mid July. The model, lagging slightly behind, clears the bay of ice by mid August. Although the model systematically lags behind satellite observations in both the growth and decay of ice, it does portray the seasonal variation of ice concentration, extent, growth and decay in a consistent and natural fashion.

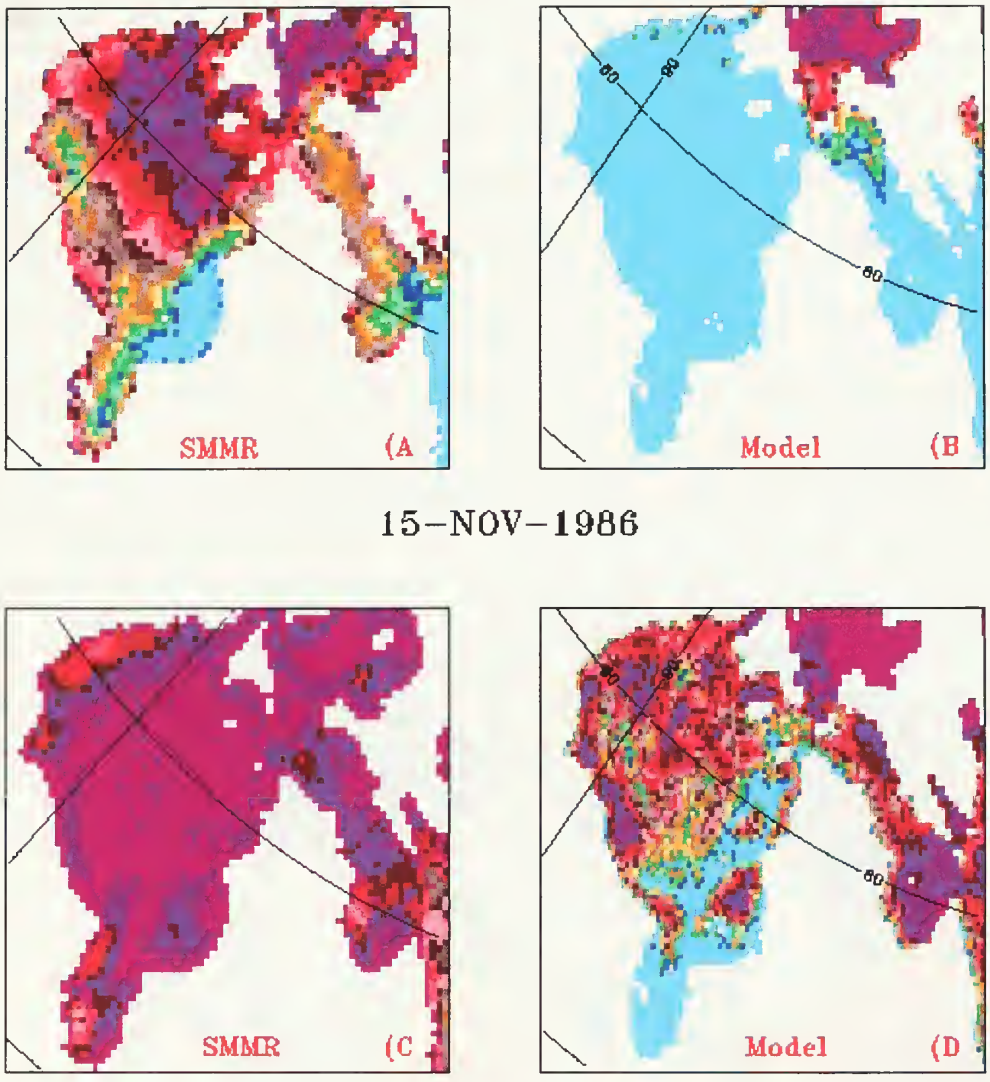

Figure 5-2. Upper frames show model ice concentration (b) lagging behind satellite observations (a) in the freezing of Hudson Bay. Lower frames depict the model (d) ice concentration one month later beginning to catch up with satellite ice concentration observations (c).

The relaxation of the ocean model surface layer to Levitus and Boyer [1994] temperature and salinity climatology appears to be related to the observed time lag in Hudson Bay. Figure 5-3 demonstrates the Levitus and Boyer temperatures for March and September are essentially the same. It appears that in order to freeze Hudson Bay, the model must wait until very cold air temperatures are available to overcome the erroneously high climatological winter temperature of 4°C.

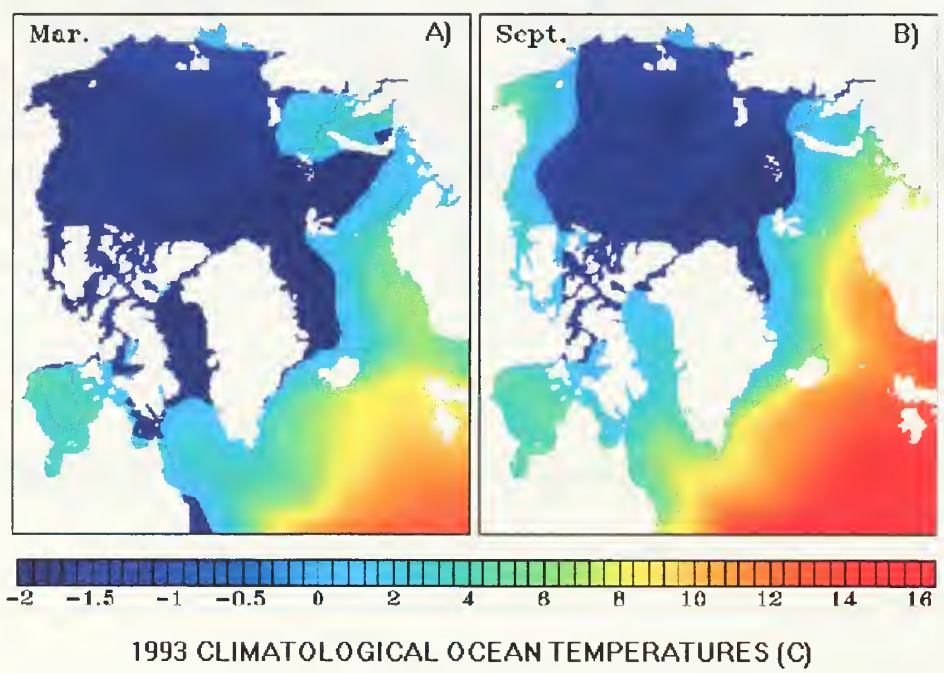

Figure 5-3. Levitus and Boyer temperatures for March (left) and September (right) 1993. The temperatures in Hudson Bay are essentially the same for winter and summer.

There is also a time lag in the model simulation of the melting of ice in Hudson Bay. The Levitus and Boyer temperatures for April through June show very little change. It is not until July that temperatures increase (Fig. 5-4). The model again appears to have to wait until July when very warm air temperatures are available to melt the ice in Hudson Bay.

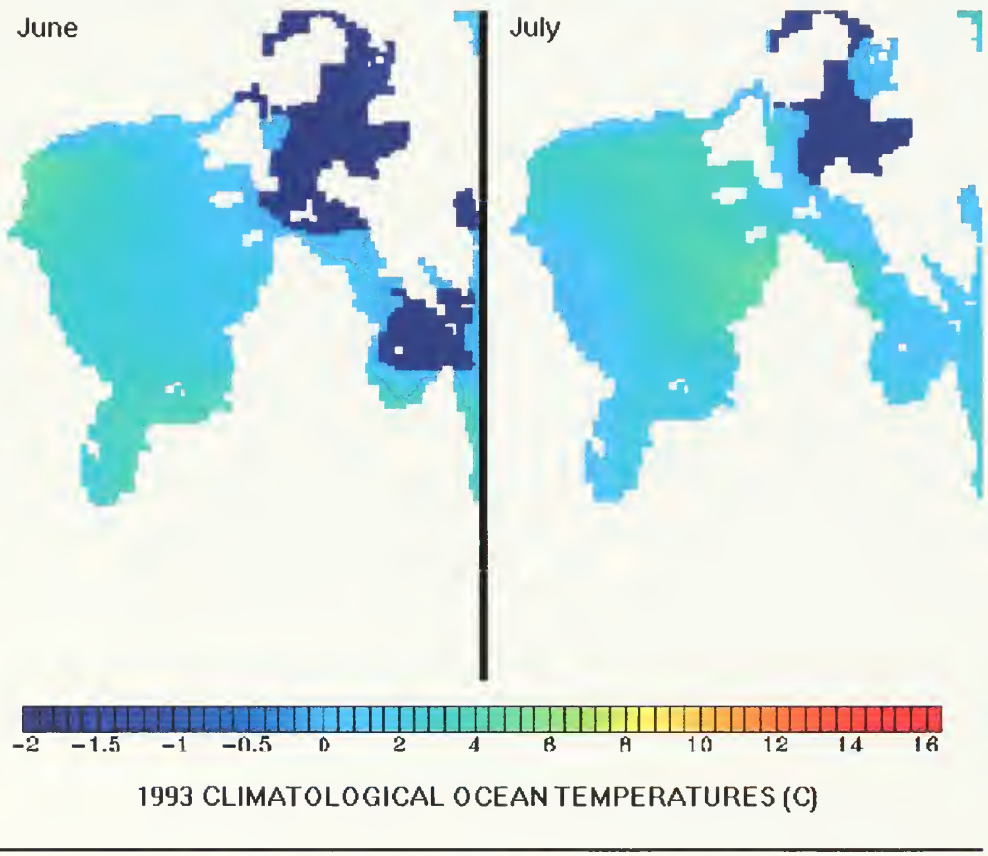

Figure 5-4. Levitus and Boyer ocean temperatures for June (left) and July (right) 1993. The figures show a delayed temperature increase in July.

In the Beaufort, Laptev, East Siberian and Chukchi Seas (Fig. 5-5) the model appears to have difficulty in melting

the ice during the summer. Ice concentration values remain nearly 100% for much of the region and don't reflect the retreat and breakup of ice along the marginal seas. Too cold historical temperatures in the summer (Fig. 5-3) are partly responsible for the model problems in this region. Russian data (Pavlov, 1996) has shown the ocean surface temperature during the summer to be as high as 5° C in these seas. Additionally, the model simulation does not take into account the input of heat and freshwater from the Russian and Alaskan rivers to these marginal seas.

Model performance in this area was also degraded by the closed boundary at the Bering Strait. The influx of heat from the Pacific was not present in the model simulation. All these factors combined to cause the model to retain excess ice in this region during the summer.

2. Small Scale Features

The seasonal variation of ice concentration depicted by the model is consistent during growth, decay and steady state. There are no apparent spurious oscillations or stair-step progressions. In the Kara and Barents Seas the model resolution was fine enough to portray small-scale features such as the reduction of ice concentration values around Franz Josef Land and Severnya Zemlya in early spring.

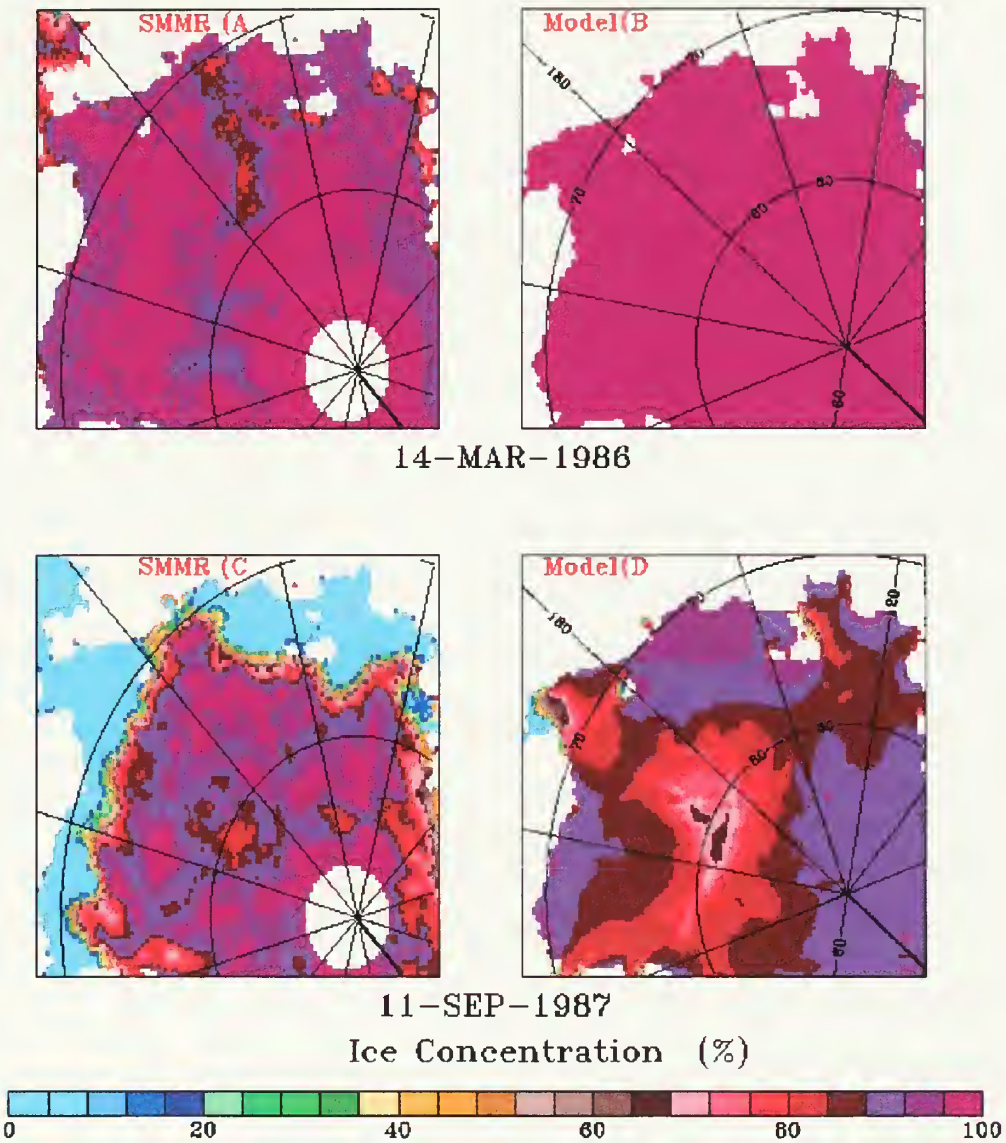

Fig. 5-5 Satellite (a,c) and Model (b,d) ice concentration for the Beaufort, Laptev, East Siberian and Chukchi Seas in winter (upper) and summer (lower). The lower panels show the model weakness in simulating the retreat of ice in these marginal seas.

The model accurately depicts the pattern of ice concentration from the southern tip of Svalbard across the northern edge of the Barents Sea to the northern tip of

Novaya Zemlya in mid December (Figs. 5-6a and b). The model has also correctly depicted the formation of ice east of Novaya Zemlya in the Kara Sea while leaving the Barents Sea to the west open. Through the winter the model continues to do well as it extends ice from the Kara Sea along the Russian coast into the White Sea as shown in Figs. 5-6c and d. The model captures the growth pattern correctly although it does lag behind observed ice growth by approximately one month.

The model also appears to over forecast the extent and concentration of ice off the eastern coast of Greenland. Even though the model tends to advect excessive amounts of ice along the eastern coast of Greenland, it does an excellent job of detailing a small-scale feature by retaining 100% ice concentration (fast ice) in Jokel-bugten with lower values to the north, east and south (Fig 5-7). This region of fast ice that the model appears to be capable of resolving is associated with the opening of the Northeast Water Polynya (Schneider and Budeus, 1995).

Although in the Hudson Bay region the model experiences a 30-day lag, it does appear to be able to resolve synoptic weather events. From 6 to 24 February 1980 (Fig. 5-8) satellite observations showed a reduction in ice concentration to 70% for a small area in the extreme

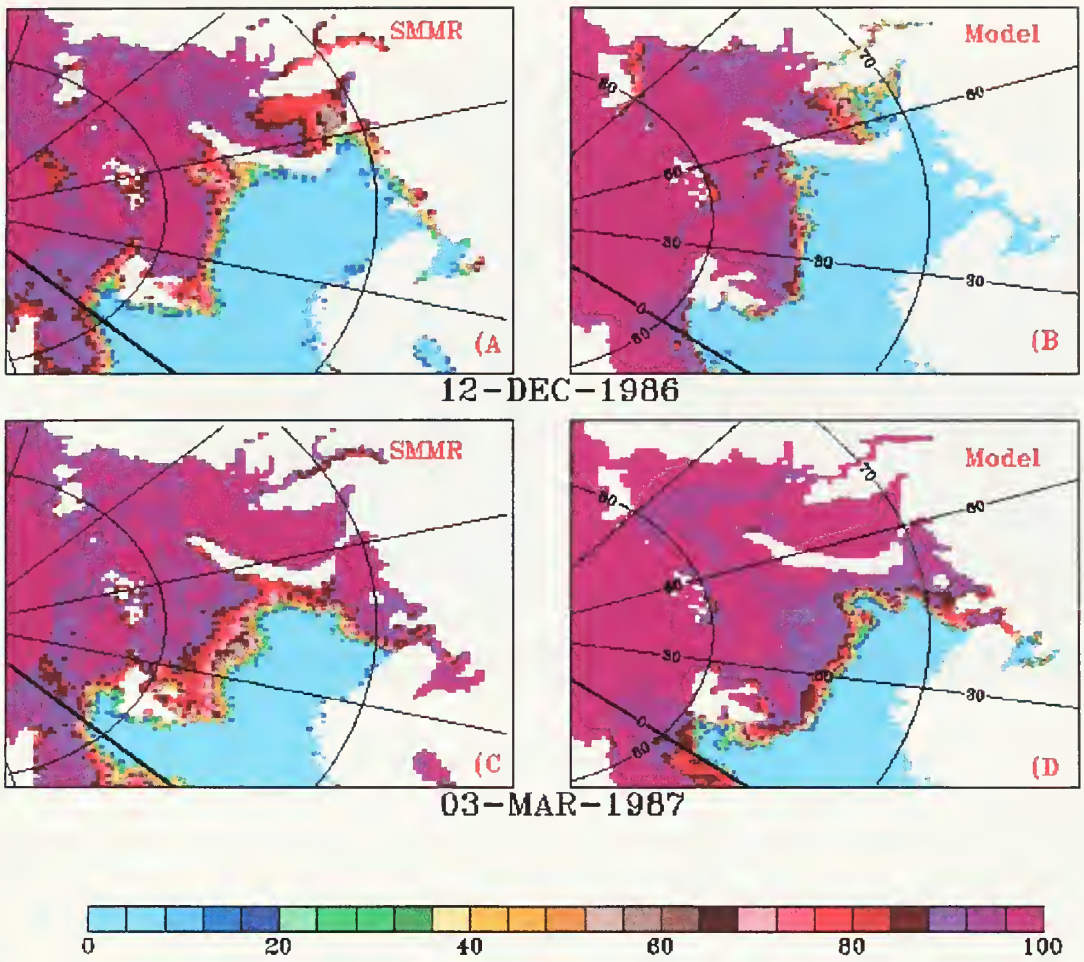

Figure 5-6. Ice concentration (%) for the Kara and Barents Seas on 12 December 1986 and 3 March 1987. The upper panels show the excellent correlation of the model (b) with satellite observations (a) in the Kara and Barents Seas during early winter. The lower panels show how the model (d) reflects observations by growing ice along the Russian coast in late winter into the White Sea.

northwest of Hudson Bay. This feature was quite evident in the model output. It appears that the model was able to resolve a small-scale weather event, as this opening in the ice was probably a wind driven event.

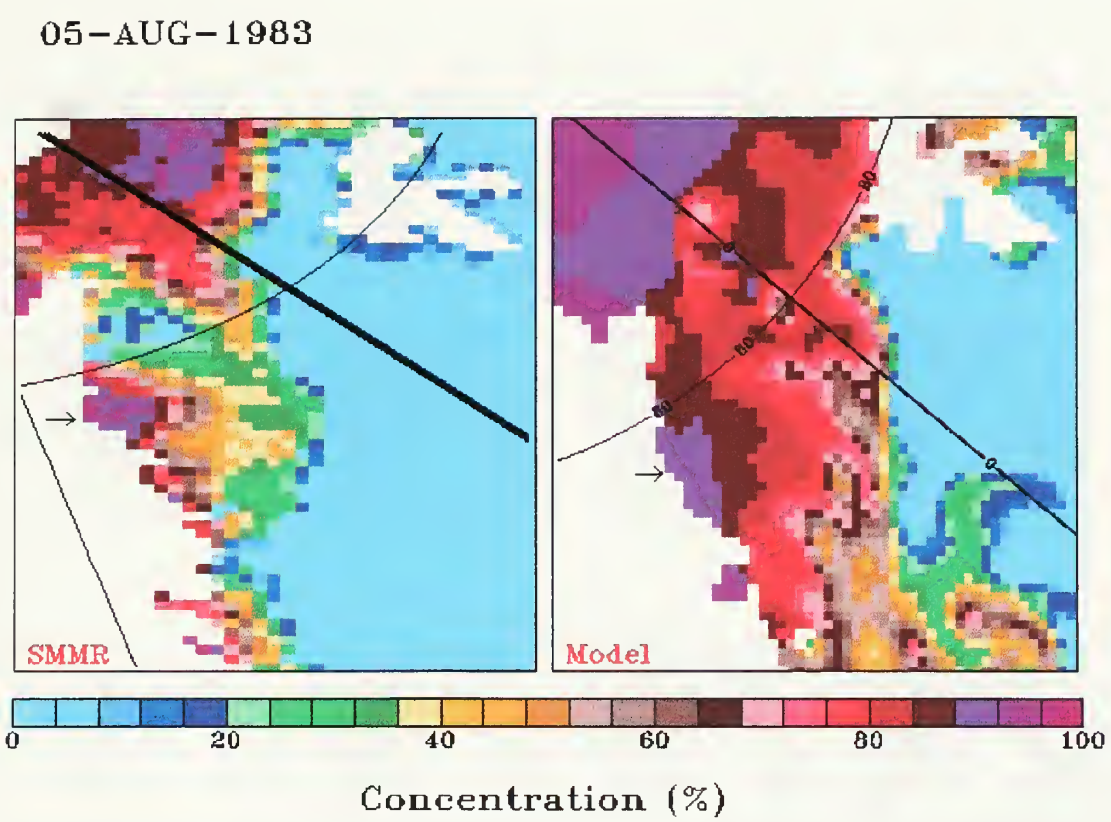

Figure 5-7. Ice concentration (%) from SMMR (left) and model (right) on August 5, 1983 showing fast ice depicted accurately by model at Jokel-bugten (indicated by arrow) on the northeast coast of Greenland.

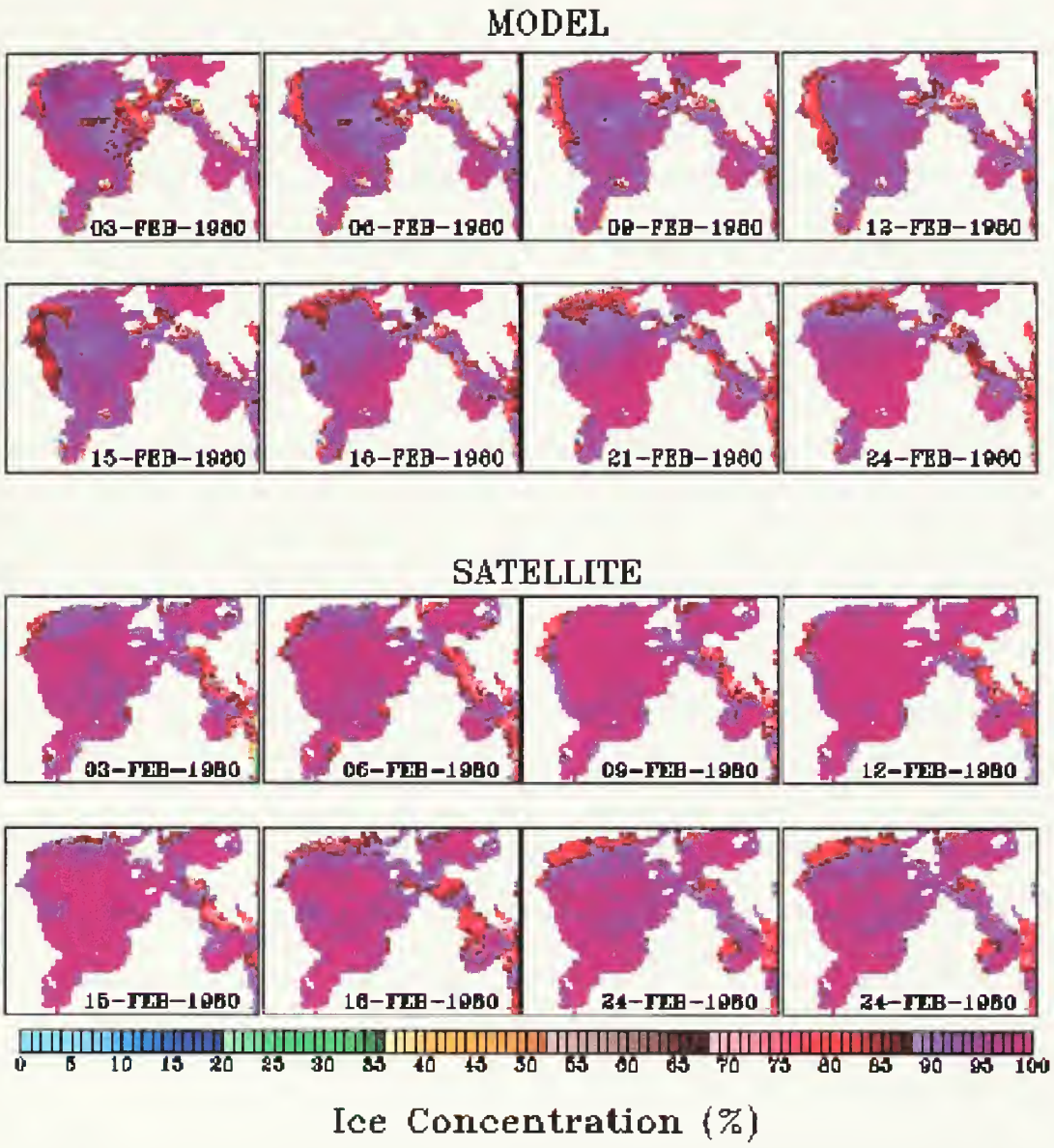

Figure 5-8. Ice concentration from the model (upper two rows) accurately depicts a small-scale opening in the northwest of Hudson Bay during the winter of 1980 as observed by SMMR (lower two rows).

B. VARIABILITY

In the side-by-side animation of the 15-year model ice concentration simulation against the satellite observations there is the readily recognizable seasonal variation of the ice concentration. However, the side-by-side animation only gives a subjective visual representation of the seasonal variation of ice growth and decay. This portion of the paper will quantify this variability statistically.

1. Variance

For each of the years the data sets were summed to determine the annual mean ice concentration at each grid point. A 15-year annual record was created for both the satellite and model ice concentration fields. The 15-year mean values were used in the calculation of the variance in ice concentration. Variance values for the satellite and model were computed as:

$$\sigma^2 = \sum_{l=1}^{l_{max}} \left(S_{i,j} - \overline{S_{i,j}}\right)^2 \Big/ \left(l_{max} - 1\right)$$

where l_{max} = the total number of timeframes in the dataset,
$S_{i,j}$ = the satellite ice concentration value at grid point i, j at each timeframe l,
and $\overline{S_{i,j}}$ = the satellite 15-year mean at grid point i, j.

$$\sigma^2 = \sum_{l=1}^{l_{max}} \left(M_{i,j} - \overline{M_{i,j}}\right)^2 \Big/ \left(l_{max} - 1\right)$$

where l_{max} = the total number of timeframes in the dataset,

$M_{i,j}$ = the model ice concentration value at grid point i, j at each timeframe l,

and $\overline{M_{i,j}}$ = the model 15 - year mean at grid point i, j.

The variance measures the total variability, including both the seasonal and interannual signals, of ice concentration over the 15 year period. In the marginal seas of the Arctic Ocean the seasonal variability is much larger than the interannual variability. Therefore, the variance in the marginal seas mainly reflects the seasonal variability. The variance comparison allows the depiction of regions where the model has successfully simulated areas of high variability and those which it has missed. Figure 5-9 shows the variance values from the model and the satellite. Both the model simulation and satellite observations show large variance in Hudson Bay, southern Baffin Bay, Barents Sea, Labrador Sea and GIN Sea, i.e., regions where there is near to complete ice melt in summer. Even though the model may lag during the melting and freezing of ice in Hudson Bay, as discussed in the previous section, the seasonal presence or absence of ice is well represented. In the Barents and GIN (Greenland-Iceland-Norwegian) Seas the large variance in the model is located farther south and east than in the

satellite observations, indicating the ice edge (extent) is too far south and east. Lower variance in the Kara Sea and northern Baffin Bay suggests the model simulation has too much ice in the summer for these regions.

In the Barents Sea the northern edge and in the GIN Sea the western edge of high variance in Figure 5-9 infers the summertime ice edge. Similarly, the wintertime ice edge is defined by the southern and eastern edges of high variance. Figures 5-10 and 5-11 depict the winter and summer ice concentrations for the Barents and GIN Seas, respectively. They illustrate that the variance plot defines the range of the ice edge advance and retreat. The model appears to oversimulate the ice extent for these two regions and the seasonal swing in the Barents Sea is smaller because the high variance area is narrower as compared to the satellite observations.

The variance plot also highlights an area of extremely high value in the Chukchi Sea in the satellite observations (Fig. 5-9a), which is not reflected in the model. Variance values in the model's Laptev, East Siberian, and Beaufort Seas are all low as compared to the satellite observations, indicating that the model fails to simulate the large seasonal variation in ice concentration for these regions,

primarily due to the erroneous climatological data, as pointed out in the previous section.

The one truly anomalous feature of the model simulation is a finger of ice extending into the North Atlantic off Nova Scotia (Fig. 5-9b). This is due to the advection of ice along the southern boundary of the model domain. The solid wall boundary condition does not allow the ice to be advected beyond it.

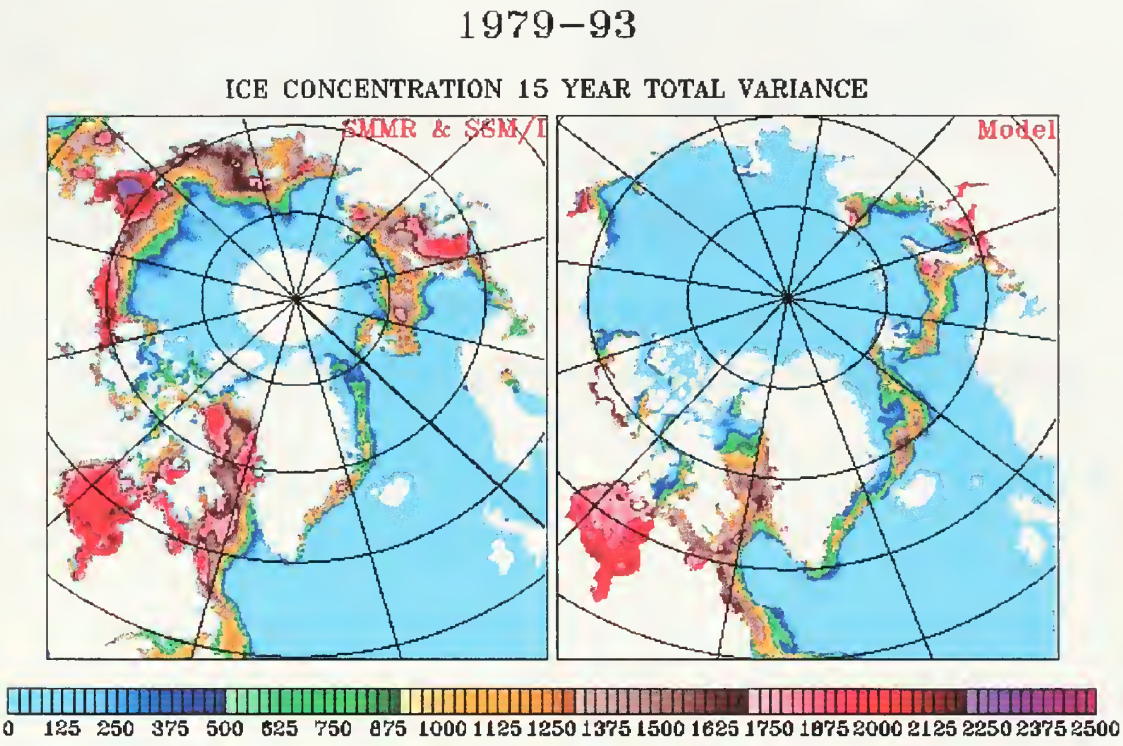

Figure 5-9. Variance for the satellite ice concentration observations (a) and model simulation (b). Favorable comparison is evident in the Barents Sea. The Beaufort, East Siberian, Chukchi and Laptev Seas all have significantly lower variance in the model simulation.

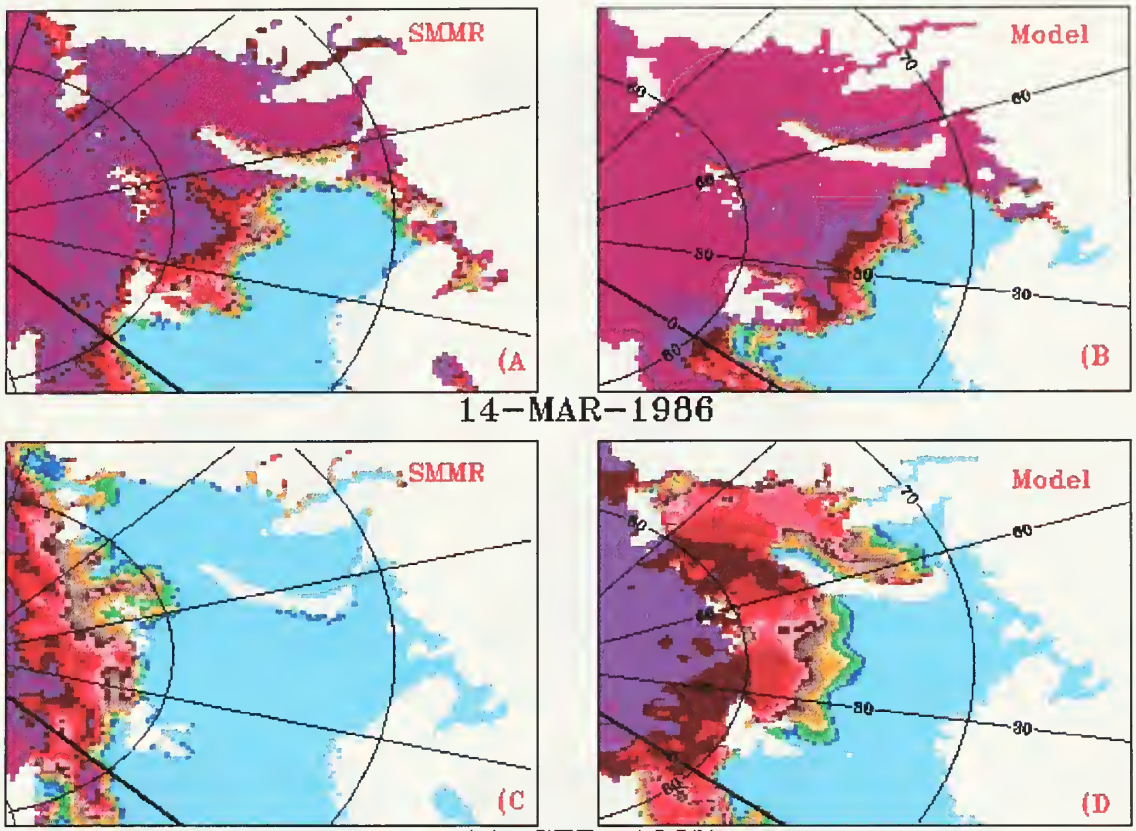

Figure 5-10. Ice concentration for satellite observations (a,c) and model simulation (b,d) in the Kara and Barents Seas. The model has overforecast the ice concentration and extent in both the winter and summer.

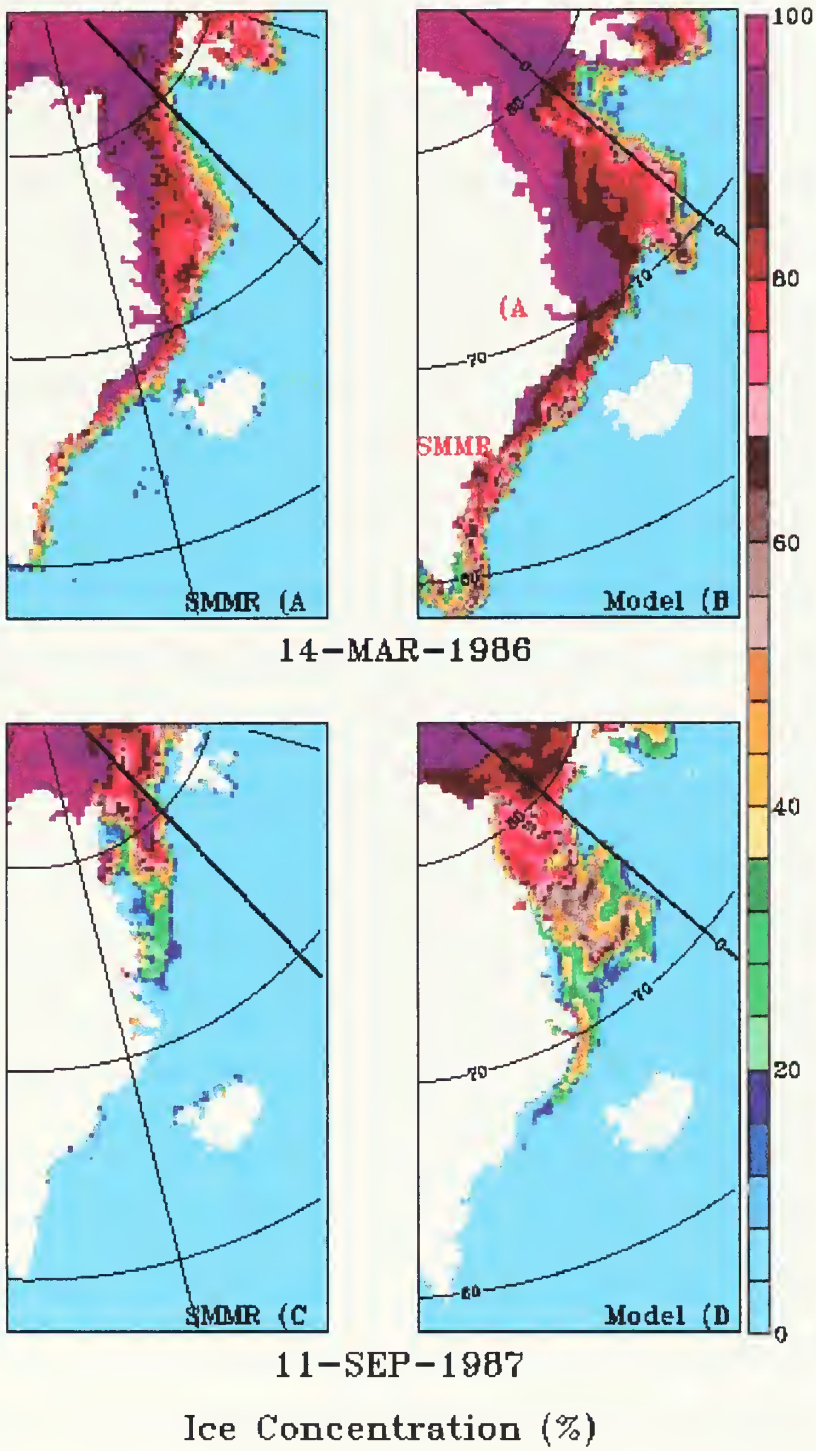

Figure 5-11. Ice concentration for satellite observations (a,c) and model simulation (b,d) in the GIN Sea. The model has overforecast the ice concentration and extent in both the winter and summer.

C. ANOMALY

The preceding two sections of this chapter have described the similarities and differences between animations of satellite observations and model simulation ice concentration and ice concentration variability. This section will use a more quantitative method. The method utilized is the comparison of the satellite data set with the model output fields by calculating an anomaly value. This method is a direct subtraction of the model output field from the corresponding satellite observation grid point. Previously the satellite data set grid of 448 X 304 was cropped to match the area of coverage used by the model grid of 361 X 301. The calculation of an anomaly field required the satellite data set to be converted to the model grid. The conversion was accomplished using a locally written Fortran routine, which used a weighted average of the four nearest satellite grid points to the model grid point. From the converted satellite data set the model data was directly subtracted to calculate the anomaly. The satellite minus model anomaly values were plotted at three-day timeframes for single and multi-year animations. The model domain has been subdivided into six geographic regions to further facilitate an in-depth comparative study. The geographic regions are depicted in Figure 5-12. Average

anomaly values for the model domain and for each sub-region were computed by averaging the anomalies of all grid points for each three-day time frame. The averaged anomaly values were then plotted as a time series with satellite minus model anomaly in x and time in y.

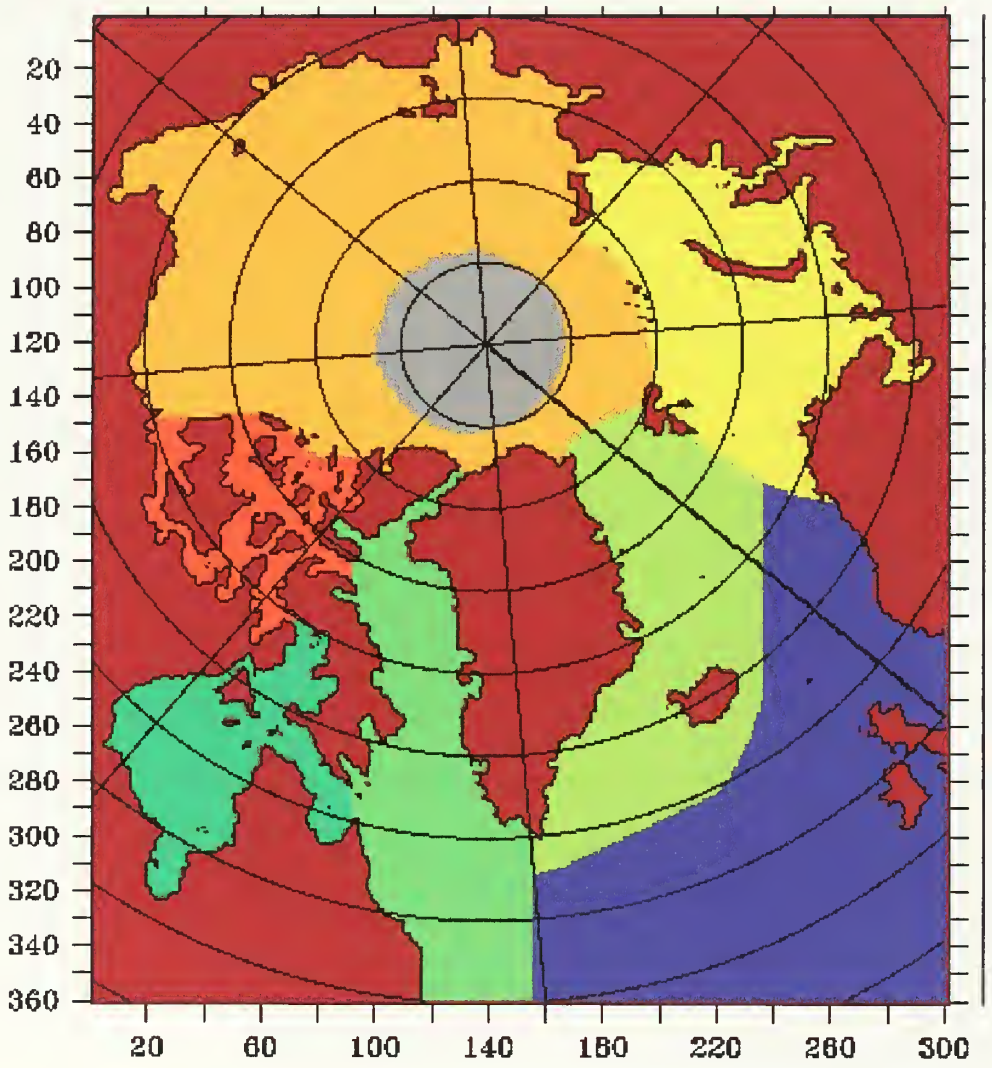

Figure 5-12. Regional breakdown of the model grid. Green is Hudson Bay, light green is Baffin Bay, lime green is the GIN Sea, yellow is Kara and Barents Seas, orange is central Arctic and pumpkin is the Canadian Archipelago.

1. Basin wide discussion of anomaly

Figure 5-13 shows the time series of ice concentration anomaly averaged over the entire model domain. Negative anomaly values are generated when the model portrays higher ice concentrations than the corresponding satellite observation and conversely. The time series of ice concentration anomaly is dominated by a strong seasonal variability. After the first four years of the simulation where a small positive anomaly occur during the winter, the seasonal variation reaches its minimum value of 0.0% in December. The anomaly value shows a steady negative increase with perturbations on the order of +-0.5% through May to approximately -6.0%. In June the anomaly undergoes a rapid negative increase to its maximum of approximately -14.0%. This maximum anomaly is maintained through September. In October the anomaly falls precipitously to about -2.0%. The remainder of the year shows a slower but steady drop in anomaly to the minimum again in December. The seasonal variation of the anomaly pattern is detailed in the lower panel of Figure 5-13 that shows the years 1990 through 1992.

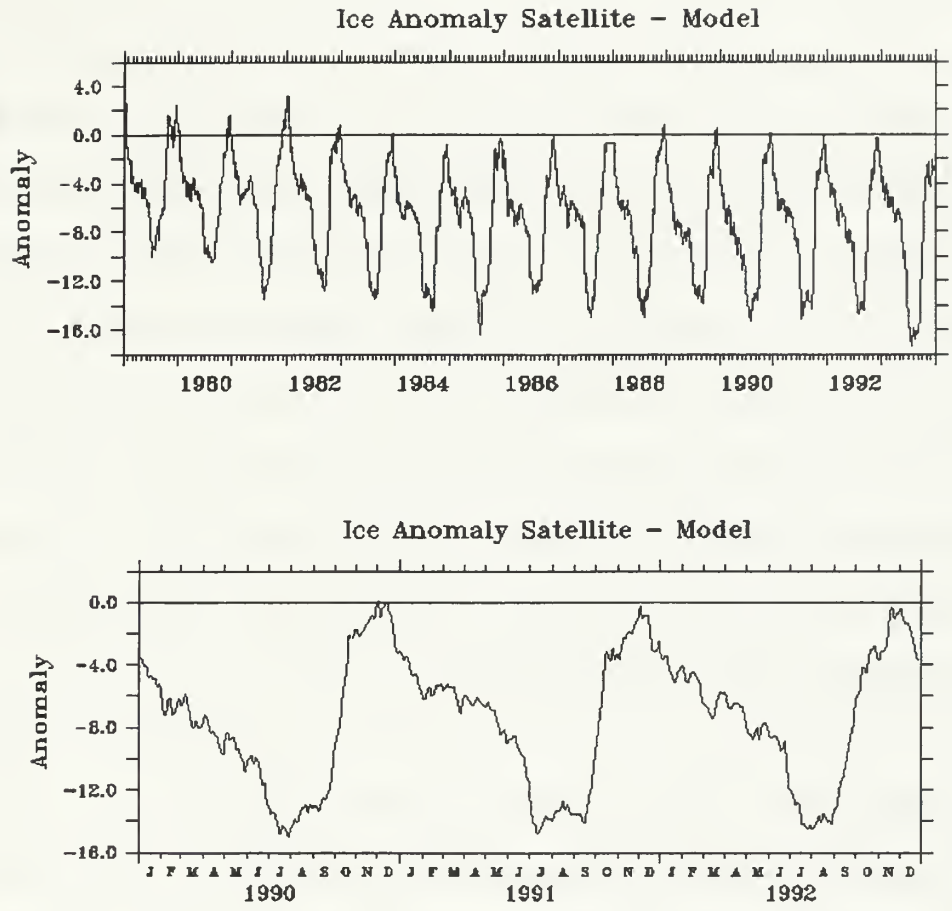

Figure 5-13. Time series of ice concentration anomaly (satellite observation minus model simulation) averaged over the entire model domain. Upper panel shows the seasonal variation over the 15-year model simulation. Lower panel provides detail on seasonal variation from 1990-92.

Anomaly values are generated when the model differs from the satellite observations of ice concentration or when the model's geographic location for the ice edge is not the same as the satellite observation. This is especially evident in the MIZ (marginal ice zone) where model concentrations of 100% can be found but for which satellite

observations report 0% ice concentrations. The maximum anomaly values in the summer appear to be a result of the models tendency to overforecast and retain too much ice along with the bias in the satellite data to underestimate ice concentration area and extent. The wintertime anomalies are much lower suggesting the model performs better and the satellite values are more accurate. Figure 5-14 gives two examples of spatial distribution of the anomaly. The anomaly values are on a scale of -100% to +100% with all values more negative than -20% plotted as sky blue and all values greater than +20% as dark purple.

The anomaly spatial distribution in December (Fig. 5-14, right panel) shows maximum anomaly values more negative than -20% in the MIZ of the GIN Sea suggesting the model has overforecast the ice extent. Meanwhile anomaly values of greater than +20% are present in Hudson Bay and the White Sea which indicates the model is late in freezing up these areas. The bulk of the central basin shows anomaly values of ~-1.6%. As the winter progresses the positive anomaly in Hudson Bay disappears (not shown) after the model catches up and freezes this region. There also continues to be a wide band of more negative than -20% anomaly along the MIZ in the GIN Sea and the Kara and Barents Seas, which suggests the model continues to overforecast the extent of ice. By May

(Fig. 5-14, left panel) most of central basin of the Arctic shows anomaly values of +-1.6%.

With extensive filaments of more negative than -20% anomaly extending east into the Atlantic off Newfoundland and south and east off the tip of Greenland are also present. The filament off Newfoundland, as previously discussed, is an artifact resulting from the no-flow boundary at the southern edge of the model domain. The filament off the southern tip of Greenland appears to be the result of excess ice being advected by the model along the coast and getting caught up in northeast moving low pressure systems.

In June through August the area containing more negative than -20% anomaly reaches its greatest extent. Hudson Bay, the Canadian Archipelago, Baffin Bay, and the East Greenland Sea all show areas of more negative than -20% anomaly in the summer. In Baffin Bay and the East Greenland Sea this strong anomaly is due to an incorrect ice edge, while in Hudson Bay and the Canadian Archipelago it suggests too high ice concentration values in the model. High concentrations in Hudson Bay may also be due to the late melting season, while in the Canadian Archipelago, ice does not ever completely melt in the model as it does in the satellite observations. Most areas of the central Arctic

show -6% to -12% anomaly during the summer. In October the central basin anomaly values reduce rapidly to about -1.6%.

The annual pattern of maximum negative anomaly in the summer is very probably not simply a function of poor model performance in the summer. It may be much in part due to the tendency (as reviewed in Chapter III) of satellite observations to underestimate the ice concentration and extent during the summer due to the presence melt ponds. The model however does appear to be slow to melt ice and to overestimate its extent. This however does not account for the entire summertime maximum anomaly that must be partially due to the lower reliability of the satellite observations during this period.

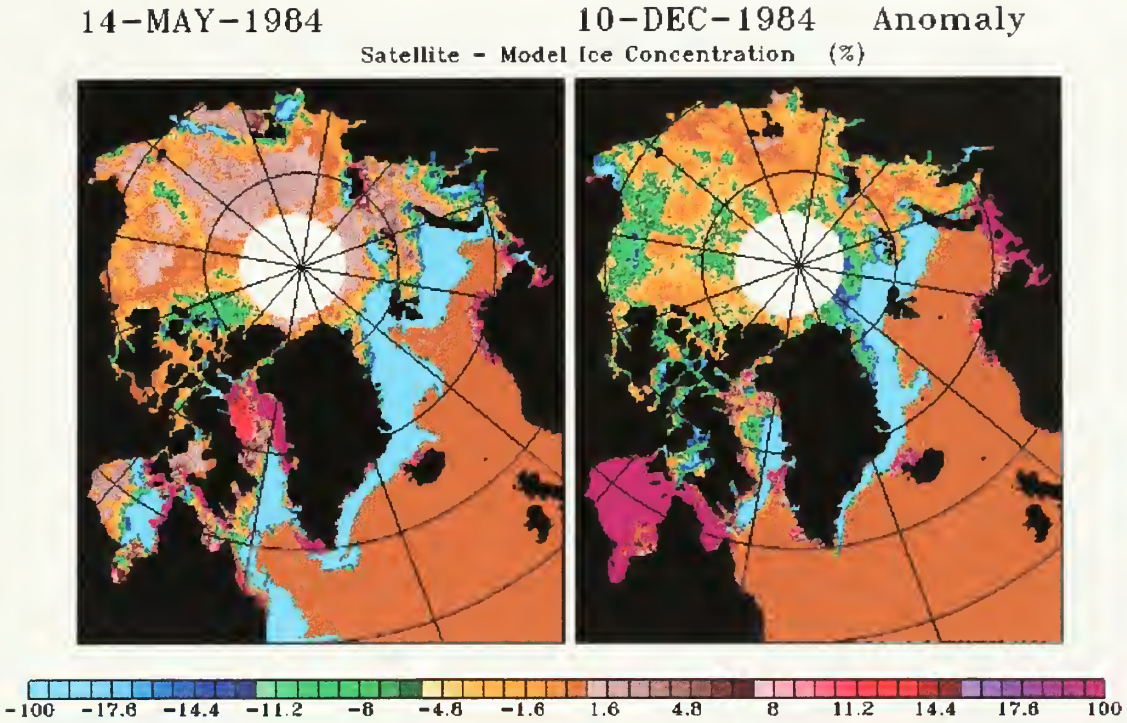

Figure 5-14. Ice concentration anomaly, satellite observations minus model output. Left panel shows negative anomaly in much of North Atlantic MIZ during late winter/early spring. Right panel shows positive anomaly in Hudson Bay and reduced extent of negative anomaly in North Atlantic MIZ in winter.

2. The Kara and Barents Seas

In the Kara and Barents Seas the averaged anomaly time series for the sub-region shows an annually repeating pattern of positive anomaly in December to a negative maximum anomaly (Figure 5-15c) in June/July. The time series shows a somewhat noisy increase in negative anomaly to a maximum in June/July. During the months of August and September a slow decline in negative anomaly prevails. This

is followed by a rapid decrease in October through zero to a maximum positive anomaly in December. The change in anomaly for the Kara and Barents Seas is in phase with the curve for the entire domain (Fig. 5-15g). The animation of satellite minus model ice concentration reveals that in October through December the area of more negative than -20% anomaly in the Barents Sea shrinks in size and retreats poleward, again suggesting that model performance in simulating the ice edge improves during the winter. The greatest anomaly is a swath of more negative than -20% extending from southern tip of Svalbard to the northern tip of Novaya Zemlya in a band parallel to the ice margin and extending about 200 km to the north, which indicates the model has extended the ice edge too far south. Anomaly figures for the entire Kara Sea remain low at near +- 1.6%. As winter advances to spring the area of more negative than -20% anomaly grows southward into the Barents Sea. In May the entire western coast of Novaya Zemlya shows more negative than -20% anomaly (Fig. 5-14, left panel). Not shown is that the animation of anomaly for June/July agrees with the time series curve in that more negative than -20% anomaly covers much of the region. Therefore, the large anomaly in summer in the Kara and Barents Seas is mainly due to an unrealistic ice edge location in the model. The model extends the ice edge too

far south in the summer. A similar conclusion can be drawn for the GIN Sea (Fig. 5-15a).

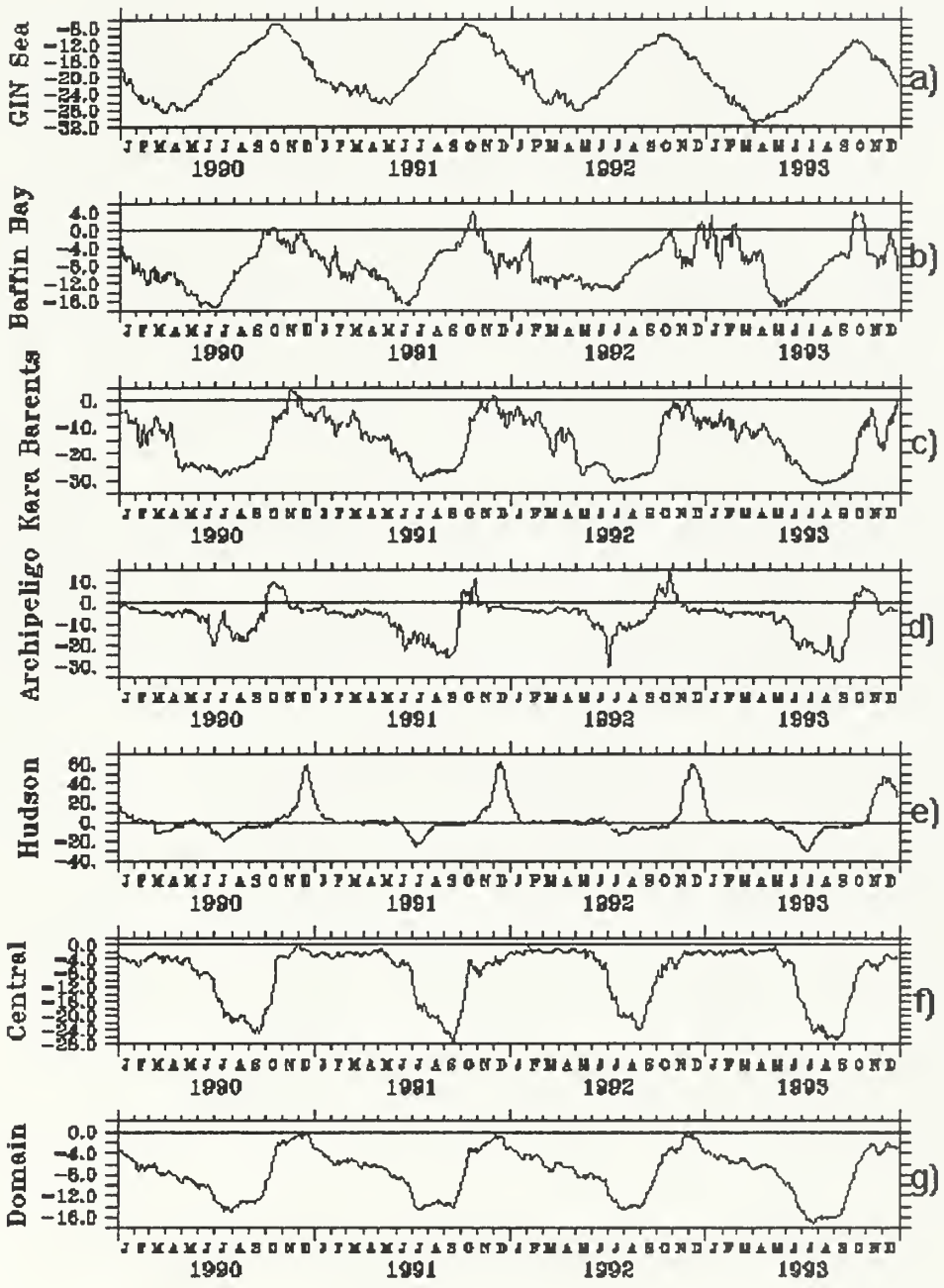

Figure 5-15. Time series of ice concentration anomaly for sub-regions (a-f) along with complete model domain (g). Sub-region boundaries are shown in Fig. 5-12.

3. Hudson Bay

In Hudson Bay the time series for the sub-region shows a distinctive annual pattern with a very high positive anomaly each December with a smaller negative anomaly in July (Fig. 5-15e). Figure 5-16 is a blow-up of panel e from Figure 5-15 to show detail. Each annual cycle has a minimum anomaly of near zero from February through June. In June a rapid increase in negative anomaly occurs. This increase continues to a maximum negative anomaly (-20%) in July that then rapidly decreases to a minimum of 4% from September till mid November. Every mid November is marked by an extremely rapid increase to a maximum of +60% anomaly. The positive anomaly rapidly falls to near zero by February.

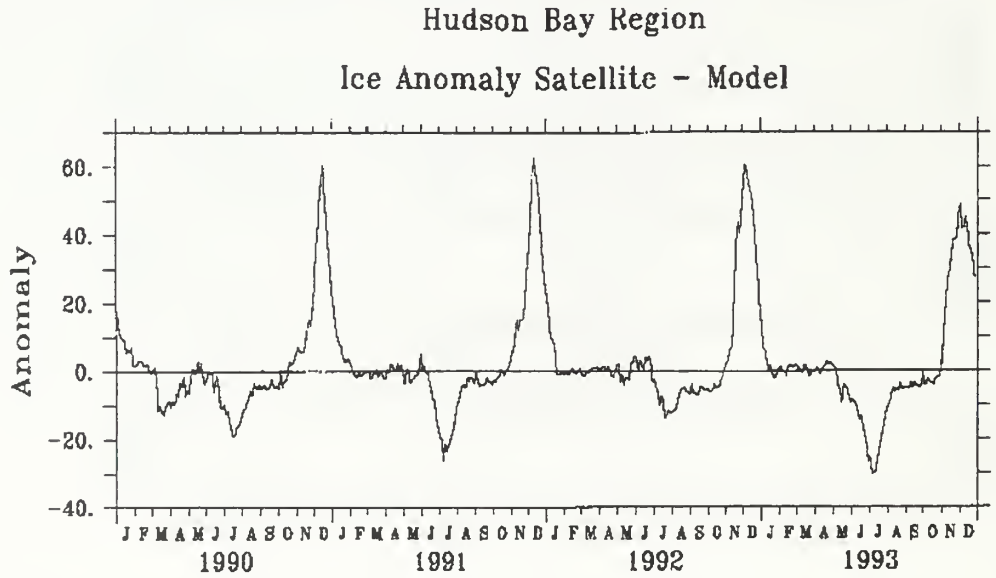

Figure 5-16 Hudson Bay sub-region anomaly curve for years 1990-93 shows strong positive anomaly peak in December followed by negative anomaly peak in July.

The anomaly animation echos the pattern demonstrated in the time series record, i.e., it shows that in August values have dropped to near zero and remain there until mid November. In December anomaly values of greater than +20% grow from the northwest towards the southeast covering all of Hudson Bay by mid December. During January the anomaly values drop to about +-2% over most of Hudson Bay with some isolated values of -8%. By late February all of Hudson Bay has dropped to 0% anomaly. This remains consistent until May when more negative than -20% anomaly covers the eastern third of Hudson Bay. This anomaly grows to cover all of Hudson Bay by July. Once again in August anomaly values drop rapidly to zero.

The time series and the animation indicate that the anomaly is directly tied to the freezing and melting cycle of Hudson Bay. In mid November Hudson Bay begins to freeze over. The model does not begin to reflect this until 30 days later. The high positive anomaly values are due to the model not growing any ice in Hudson Bay until well after satellite observations have shown it to be there. Again in early summer the melting of Hudson Bay ice is late in the model simulation. This results in high negative anomaly values

since the model retains more ice than is present in the satellite observations.

The lag in the models freezing and melting of ice in Hudson Bay appears to be due to a correction factor built into the model. This is the relaxation of the surface layer in the ocean model to inaccurate Levitus and Boyer salinity and temperatures on a 90 day time scale. The climatological temperatures for Hudson Bay in the winter (4 C) are much too high and in the summer do not warm until very late (August). It is expected that by correcting the climatological temperature data, the model's depiction of Hudson Bay during the transitional seasons would improve dramatically. By reducing or eliminating the delay in the model's freezing and melting of ice, anomaly values for Hudson Bay would be drastically reduced.

4. The Arctic Ocean

The anomaly time series for the central Arctic Ocean sub-region (Fig. 5-15f) which includes the Laptev, East Siberian and Chukchi Seas (Fig. 5-12) shows a distinctive annual pattern with a -4% minimum for most of the year with a maximum anomaly of -22% in July/August. The animation of anomaly shows that the model has overforecast both the extent and concentration of ice in the marginal seas. The high summer anomaly values are a combination of the model's

weak portrayal of the break-up and retreat of ice in the marginal seas along with the satellite bias to underprediction of ice concentration due to melt ponding.

D. DISCUSSION

The model provides an excellent tool to study global climate and the Arctic region to which it is so closely tied. The realistic portrayal of ice growth, advection, concentration and decay are indicative of the model's strength in simulating the Arctic environment. The model has the skill to resolve small-scale features and events such as the wind driven openings in the ice.

Although the model tendency is to overestimate ice concentration and extent, it still shows skill in representing the relative pattern of ice concentration. The high anomaly values in the summer are not indicative of poor model performance but rather are due largely to the underestimation of ice concentration by the satellite due to contamination from liquid water on the ice surface. Better indicators of model accuracy are the wintertime anomaly values, which, for the entire model domain are approximately 5%.

The model overestimates ice concentration in the one third of the Arctic from 120° West to 120° East. Ice

concentration and extent suggest the model is allowing too much ice to grow here. This may be due to inaccurate modeling of the input variables, which would act to restrict the growth of ice. It appears that heat and freshwater from river input along the margins of the Arctic is not well accounted for by the model. The Alaskan and Russian rivers that flow into this part of the Arctic significantly impact the growth and decay of ice for this region. Additionally, Bering Strait is a closed boundary in the model, accepting no flow. By not allowing for the inputs from the Pacific the model will not completely account for processes which would act to restrict the growth of ice and add to the decay.

The time lag of 30 days observed in the models simulation of the freezing and melting of ice in Hudson Bay appears to be a result of the correction factor which effects a relaxation of the surface layer in the ocean model to Levitus and Boyer (1994) salinity and temperatures. The climatological database for Hudson Bay contains erroneous values that are unseasonably high, e.g., in February water temperatures are 4° C. This appears to make the model slow in growing ice as it must wait until extremely low air temperatures are available to overcome the high surface temperature in the water. Additionally, the utilization of the monthly mean temperature, although weighted daily, may

still introduce high values from early in the month. This effect is magnified during seasonal transition periods where temperatures at the beginning of the month may deviate significantly from the mean due to very low temperatures later in the period. The combined effect appears to retard both the freezing and melting of ice in the marginal seas of the Arctic Ocean with the most readily evident differences visible in Hudson Bay. Climatological temperatures for the East Siberian and Laptev Seas are also inaccurate. This is a likely contributor to the weaker performance of the model in this area.

The anomalous filament of ice advected by the model off the coast of Newfoundland into the open North Atlantic is a boundary effect. The finite boundary of the ocean model does not adequately allow heat to be transferred and which would act to restrict the advection of ice southward. The southern boundary of the model allows no transport of ice across it. The ice is simply deflected east.

It appears that the finite boundaries of the coupled ice-ocean model affect the growth and decay of ice. Without the correct transfer of heat poleward the ocean model appears to allows excess ice to be grown and for decay of ice to be slowed.

VI. CONCLUSIONS AND RECOMMENDATIONS

A. CONCLUSIONS

Numerical models have proven integral to the study of global climatology. Sea ice models are critical to the improvement of general circulation models used to study the global climate. The object of this study is to evaluate a high resolution sea ice model by comparing it to derived measurements from SMMR and SSM/I satellite observations. Utilized for this study was the NASA Goddard Space Flight (GSFC) Sea Ice Concentration Data Set from the National Snow and Ice Data Center. Using animations of side-by-side presentations, variablity comparisons and anomaly values of the simularities and differences between the model and the satellite were noted.

The model consistently compares well with the satellite observations for the overall patterns of growth, decay, extent and concentration. A natural progression of growth and advection of ice in the fall and into the winter followed by decay and shrinking in the ice cover in summer is depicted by the model simulation. The model does well in its realistic depiction of ice concentration values. With values increasing poleward and decreasing equatorward. The

model's resolution and skill enable it to recognize small-scale features such as the wind driven opening in Hudson Bay and the retention of fast ice at Jokel-bugten off the east coast of Greenland. The realistic simulation of ice in the Kara and Barents Seas suggest good model skill for these regions. The physical processes governing the interactions between the North Atlantic and the Barents Sea appear to be well modeled.

The model is consistent in its depiction of ice concentration. Model ice concentration values transition smoothly while increasing and decreasing. Satellite observations are sometimes not as consistent with noisy irregular increases and decreases in ice concentration.

The differences observed between the model simulation and satellite observations indicate that the model overestimates and retains ice too long in the marginal seas of the Arctic Ocean. In this regard the model is weak in its depiction of the Laptev, East Siberian and Chukchi Seas. Model representation of the marginal seas is weak where riverine input is significant. Additionally, the Bering Strait is modeled a closed boundary that may also contribute to the model's weaker performance in this area.

Overall the model tends to over-forecast the extent of ice along the margins of the Arctic. The largest differences

are noted during the summer when high anomaly values are observed over much of the marginal seas of the Arctic Ocean. The high anomaly values in the summer are due in part to underestimation of ice concentration by the satellite due to inability to differentiate open water from melt ponds.

The model simulation lags behind observations in the thawing and freezing of ice in Hudson and Baffin Bays. The growth of ice in the late fall and early winter is delayed in the model by about 30 days. In Hudson Bay satellite observations show that by mid November ice has begun to grow from the northwest towards the southeast. The model repeats this pattern but not until mid December. This feature of the model is also evident in Baffin Bay and the other margins of the Arctic to a lesser extent.

The model has unnatural filaments of ice extending eastward into the Atlantic off the tip of Greenland and Newfoundland. This feature in the model shows ice being advected down the coast of Newfoundland and then eastward into the North Atlantic. It appears that the ice encounters the southern boundary of the model domain and being blocked to the west by land it turns east along the path of least resistance. The advection of ice down the eastern coast of Greenland and into the Atlantic produces long filaments of ice extending into the North Atlantic.

B. RECOMMENDATIONS

The focus of this study was to examine the model simulation of the Arctic Ocean and hopefully provide some recommendations for its improvement. Future model simulations could benefit by considering the suggestions of this paper.

The climatological database used by the model is likely causing problems such as the 30 day time lag observed in Hudson Bay and the other margins of the Arctic. The ocean surface layer relaxation to Levitus scheme may need to be improved or changed to another method.

The riverine input to the Arctic plays a significant role. In order for a model simulation to have superior skill these inputs must be accounted for. Improvements in the model parameterization of heat and freshwater fluxes from Arctic rivers will undoubtedly yield results. This area would also benefit from the opening of Bering Strait to allow for the proper heat flux from the Bering Sea.

The finite boundary of the ocean model used in this simulation is likely responsible for the anomalous filaments of ice advected off Newfoundland into the open North Atlantic. A global ocean model would better handle the correct treatment of heat flux towards the pole. Subsequent model simulations have shown that the use of a global ocean

model has eliminated the problem of excess ice being advected south (personal conversation Zhang, 1998).

Finally the model's resolution may not be fine enough to properly capture ocean heat transports. Because of their small radius of deformation, ocean currents may be reduced by the model, resulting in inaccurate heat transports. Inadequate transfer of heat to the ice margins may be responsible for some of the ice edge errors. Increased model resolution is anticipated to better resolve ocean currents and thereby improve model simulation of the ice edge.

LIST OF REFERENCES

Aagaard, K., and E.C. Carmack, The Arctic ocean and climate: a perspective in The Polar Oceans and Their Role in Shaping the Global Environment, pp. 5-20, edited by O.M. Johannessen, R.D. Muench, J.E. Overland, vol. 85, 1994.

Written statement of Admiral Jeremy M. Boorda, U.S. Navy, Chief of Naval Operations before the Joint Hearing Subcommittee on Military Research and Development, Committee on National Security, U.S. House of Representatives On Dual-Use Oceanographic Partnerships, 25 January 1996.

Cavalieri, D.J., NASA sea ice validation program for the Defense Meteorological Satellite Program special sensor microwave imager, J. Geophys. Res, 96, 21,969-21,970, 1991.

Cavalieri, D.J., and C.T. Swift, NASA sea ice and snow validation plan for the Defense Meteorological Satellite Program, special sensor microwave imager; NASA Tech Memo. 100683, 77 pp., 1987.

Cavalieri, D.J., J.P. Crawford, M.R. Drinkwater, D.T. Eppler, L.D. Farmer, R.R. Jentz, and C.C. Wackerman, Aircraft active and passive microwave validation of sea ice concentration from the Defense Meteorological Satellite Program special sensor microwave imager, J. Geophys. Res., 96, 21,989-22,008, 1991.

Gloerson, P., and D.J. Cavalieri, Reduction of weather effects in the calculation of sea ice concentration from microwave radiance, J. Geophys. Res., 91, 3913-3919, 1986.

Gloerson, P., W.J. Campbell, D.J. Cavalieri, J.C. Comiso, C.L.Parkinson, and H.J. Zwally, Arctic and Antarctic sea ice, 1978-1987: satellite passive-microwave observations and analysis, NASA SP-511, 1992.

Hunke, E. C., and J. K. Dukowicz, An elastic-viscous-plastic model for sea ice dynamics, J. Phys. Oceanogr., 27, 1849-1867, 1997.

Killworth, P.D., D. Stainforth, D.J. Webb, and S.M. Paterson, The development of a free-surface Bryan-Cox-

Semtner ocean model, J. Phys. Oceanogr., 21, 1333-1348, 1991.

Levitus, S., Climatological atlas of the world ocean, NOAA Prof. Pap. 13, U.S. Dept. of Commer., Washington, D.C., 1982.

Levitus, S., and T.P. Boyer, World ocean atlas 1994, vol. 4, temperature, NOAA Atlas NESDIS 3, U.S. Dept. of Commer., Washington, D.C., 1994.

Maslowski, W., Advanced modeling of the Arctic Ocean and sea ice in support of global climate studies, in Workshop on Polar Processes in Global Climate, pp. 93-96, American Meteorological Society, 1997.

Mitchell, J.F.B., S. Manabe, V. Meleshko, and T. Tokioka, Equilibrium climate change - and its implications for the future, in Climate Change The IPCC Scientific Assessment, pp. 135-162, edited by Houghton, J.T., G.J. Jenkins, and J.J. Ephraums, 1990.

Parkinson, C.L., and W.M. Washington, A large-scale numerical model of sea-ice, J. Geophys. Res., 84, 311-337, 1979.

Parsons, A.R., On the Barents Sea polar front in summer and the interpretations of the associated regional oceanography using an Arctic Ocean circulation model, Ph.D. dissertation, Naval PostGraduate School, Monterey, CA, 1995.

Pavlov, V.K., L.A. Timokhov, G.A. Baskakov, M.Y. Kulakov, V.K.Kurazhov, P.V. Pavlov, S.V. Pivovarov, and V.V. Stanovoy, Hydrometeorological regime of the Kara, Laptev, and East-Siberian Seas, Tech. Memo. TM 1-96, App. Phys. Lab., Univ. of Wash., Seattle, 1996.

Randall, D.,J. Curry, D. Battisti, G. Flato, R. Grumbine, S. Hakkinen, D. Martinson, R. Preller, J. Walsh, and J. Weatherly, Bulletin of the AMS, 79, 197-219, 1998.

Schneider, W., and G. Budeus, On the generation of the Northeast Water Polynya, J. Geophys. Res., 100, 4269-4286, 1995.

Semtner, A. J., A model for the thermodynamic growth of sea-ice in numerical investigations of climate, J. Phys. Oceanogr., 6, 379-389, 1976.

Semtner, A. J., and R. M. Chervin, Ocean general circulation from a global eddy-resolving model, J. Geophys. Res., 97, 5493-5550, 1992.

Steffen, K., and A. Schweiger, NASA team algorithm for sea ice concentration retrieval from Defense Meteorological Satellite Program special sensor microwave imager: comparison with Landsat satellite imagery, J. Geophys. Res., 96, 21,971-22,987, 1991.

INITIAL DISTRIBUTION LIST

1. Defense Technical Information Center 2
   8725 John J. Kingman Rd., STE 0944
   Ft. Belvoir, VA 22060-6218

2. Dudley Knox Library 2
   Naval Postgraduate School
   41 Dyer Rd.
   Monterey, CA 94943-5101

3. Professor Robert H. Bourke 2
   Chairman, Department of Oceanography, Code OC/Bf
   Naval Postgraduate School
   Monterey, CA 93943-5000

4. Professor Albert J. Semtner 1
   Department of Oceanography, Code OC/Se
   Naval Postgraduate School
   Monterey, CA 93943-5000

5. Research Associate Professor Yuxia Zhang 1
   Department of Oceanography, Code OC/Zh
   Naval Postgraduate School
   Monterey, CA 93943-5000

6. Research Assistant Professor Wieslaw Maslowski 1
   Department of Oceanography, Code OC/Ma
   Naval Postgraduate School
   Monterey, CA 93943-5000

7. LT Stephen Murley, USN 1
   Department of Oceanography
   Naval Postgraduate School
   Monterey, CA 93943-5000

8. Commanding Officer 5
   Fleet Numerical Meteorology and Oceanography Center
   Attn: LT David S. Dimitriou, USN
   7 Grace Hopper Ave, Stop 2
   Monterey, CA 93943